7

Microphysics parameterizations

7.1 Introduction

As discussed more fully in the previous chapter, moist convection plays a very important role in the atmosphere. Moist convection is a key link in the El Niño Southern Oscillation that influences global circulation patterns, while organized mesoscale regions of convection are also known to modify the local and large-scale environments across the globe. Moist convection produces clouds, some of which can persist for days, influencing the absorption and scattering of solar radiation and the absorption of terrestrial radiation. Clouds also affect the concentration of aerosol particles through scavenging, precipitation, and chemical interactions.

Cloud formation is accomplished primarily by upward vertical air movement in cloud-free regions leading to patches of air that have relative humidities in excess of 100%. Once the relative humidity is above 100%, cloud droplets can form producing clouds. The microphysical processes that govern cloud particle formation, growth, and dissipation on very small scales play an important role in how moist convection develops and evolves. Cloud microphysical processes are very important to predictions of the atmosphere at temporal scales ranging from minutes to centuries, owing to the effects of latent heat release due to the phase changes of water and the interactions between clouds and radiation (GEWEX 1993).

Cloud microphysical processes represent an important uncertainty in climate modeling. Increases in aerosols due to either anthropogenic or natural causes produce an increase in cloud droplet concentration. For a fixed liquid water content, this leads to a decrease in droplet size and to an increase in cloud optical thickness and hence cloud albedo (Twomey 1977). This is particularly important over the oceans where there are fewer aerosols. However, the decreased cloud droplet size also reduces the precipitation efficiency, thereby

increasing the cloud liquid water content, cloud thickness, and cloud lifetime (Albrecht 1989). Some aerosol particles also act to decrease cloud reflectance (Kaufman and Nakajima 1993). These indirect aerosol effects strongly influence fractional cloudiness and albedo, producing a net cooling effect, yet they represent one of the largest uncertainties in studies of global climate change. An added complication arises due to the aerosol particle chemical composition being important to its activation as a cloud droplet (Shulman *et al.* 1997; Raymond and Pandis 2002), although activation appears to be mainly determined by aerosol particle size (Dusek *et al.* 2006).

Cloud microphysical processes also are important to very short-lived atmospheric phenomena, such as thunderstorms. Brooks *et al.* (1994a, b) suggest that the strength and lifetime of low-level mesocyclones (a rotating vortex of 2–10 km diameter within a convective storm) are a function of the balance between outflow development and low-level baroclinic generation of vorticity. Outflow strength is determined by the evaporation of precipitation falling from the convective storm and thus is a key factor in low-level mesocyclones that can produce tornadoes. While microphysical processes are involved in all aspects of the storm lifecycle, this example highlights how the processes that occur at the molecular scale alone can influence much larger phenomena.

These studies highlight the need to include microphysical processes within numerical weather prediction models. As model grid spacing decreases, it becomes possible to model cloud development and evolution explicitly by incorporating additional equations into a model that represent the various water substance phases and cloud particle types. This is referred to as an explicit microphysics parameterization, in which clouds and their associated processes are represented directly on the model grid. This parameterization approach contrasts with convective parameterization, where only the cumulative effects of clouds are represented on the grid (an implicit parameterization). It is generally believed that moving away from convective parameterization toward the explicit representation of cloud processes is beneficial, although many uncertainties have yet to be explored fully.

The distinction between implicit and explicit parameterization of cloud processes is often blurred in actual models. As discussed in Chapter 6, many models that are run at 10 40 km grid spacing use some combination of convective parameterization and explicit cloud microphysics parameterization. The convective parameterization scheme activates deep convection prior to the occurrence of water vapor saturation at a grid point, while the resolvable-scale model equations are assumed to develop the appropriate larger than convective-scale precipitation processes. Thus, the implicit and explicit representations of convection act in combination to produce the convective activity.

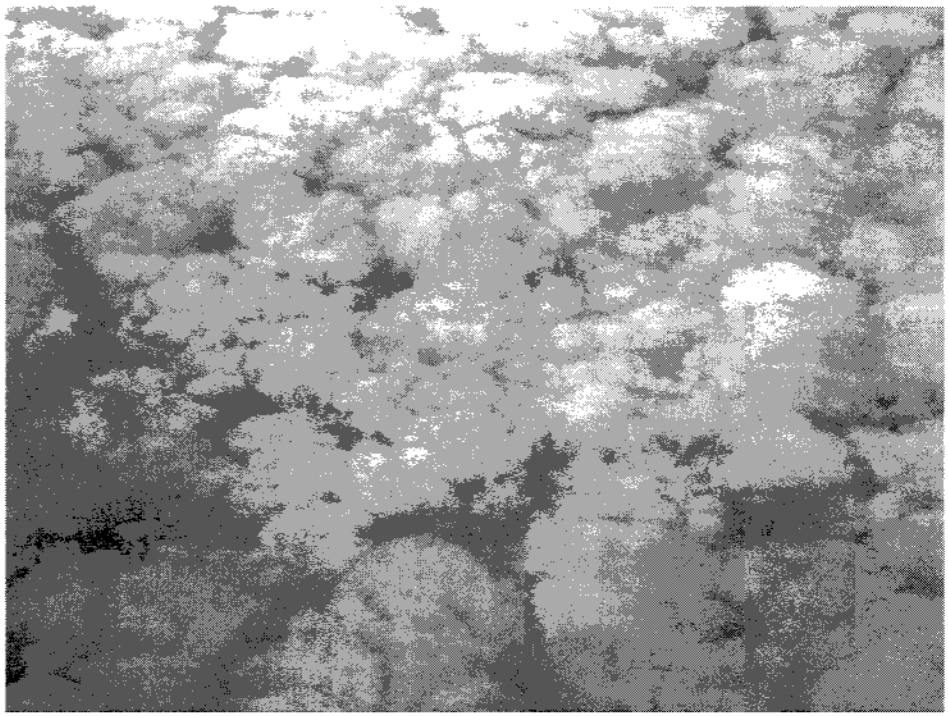

Figure 7.1. Stratocumulus clouds observed over Massachusetts photographed from a jet airplane. Notice the apparently repeatable patterns within features that are highly irregular.

Zhang *et al.* (1988) show that using both implicit and explicit schemes is a good method for handling mixed convective and stratiform precipitation systems and does not lead to double counting the heating or moistening produced by convection.

Since clouds are highly irregular, fractal entities (see Fig. 7.1), one wonders at what model grid spacing clouds can be resolved accurately. Weisman *et al.* (1997) suggest that 4 km grid spacing is just sufficient to resolve the circulations associated with squall lines. However, for predictions that include isolated thunderstorms, results from experimental model runs at 4 km grid spacing produced for the NOAA Storm Prediction Center (SPC) indicate that a 4 km grid spacing is too large. The convection produced at 4 km tends to develop upscale quickly, thereby producing too many organized convective systems when compared with observations. These results suggest that the largest grid spacing at which clouds may be accurately represented is unknown. While it is certainly less than 4 km, the behavior of thunderstorms is known to change as the grid spacing is decreased from 2 km to 500 m

(Adlerman and Droegemeier 2002) and the behavior of squall lines is known to change as the grid spacing is decreased from 1 km to 125 m (Bryan *et al.* 2003). While these behavioral changes may not greatly modify the cloud properties of the thunderstorm or squall line, they certainly modify the evolution of features that are important to severe weather warning operations, such as mesocyclones and gust fronts. Thus, it is likely that the required grid spacing is strongly tied to the atmospheric phenomena one wishes to predict. For example, very small grid spacing may be needed to predict the detailed evolution of rainfall from a precipitating mesoscale convective system. Only time and experience will yield the guidance needed to make good decisions regarding grid spacing choices.

Numerical modelers are moving quickly to incorporate microphysics parameterization schemes in models as the grid spacing goes below about 30 km. Whether these schemes are part of a hybrid approach that includes convective parameterization or a completely explicit approach, there is a need to include microphysics parameterizations in most operational forecast models in use today. Model developers face considerable challenges in their efforts to implement microphysics parameterization schemes that are both realistic and computationally affordable.

Two challenges to microphysics parameterizations are the number of phase changes of water, and the number of different interactions between cloud and precipitation particles that must be considered. The phase changes of water that can occur in the atmosphere are

vapor → liquid (condensation)
liquid → vapor (evaporation)
liquid → solid (freezing)
solid → liquid (melting)
vapor → solid (deposition)
solid → vapor (sublimation)

and do not occur at thermodynamic equilibrium. Instead, the forces of surface tension for water drops and the surface free energy for solid particles must be taken into account. To illustrate the second challenge, imagine being in an elevator with glass walls moving upward from the ground surface underneath a severe thunderstorm. Large raindrops and hail are hitting the elevator as it sits on the ground. As the elevator begins to move upward, the hail and rain persist, but raindrops of somewhat smaller sizes are also seen. At the cloud base, a dramatic transition occurs in that tiny cloud droplets are everywhere and act to obscure visibility. It is still raining and hailing, but the variety of sizes of these cloud particles is overwhelming. As the elevator moves higher

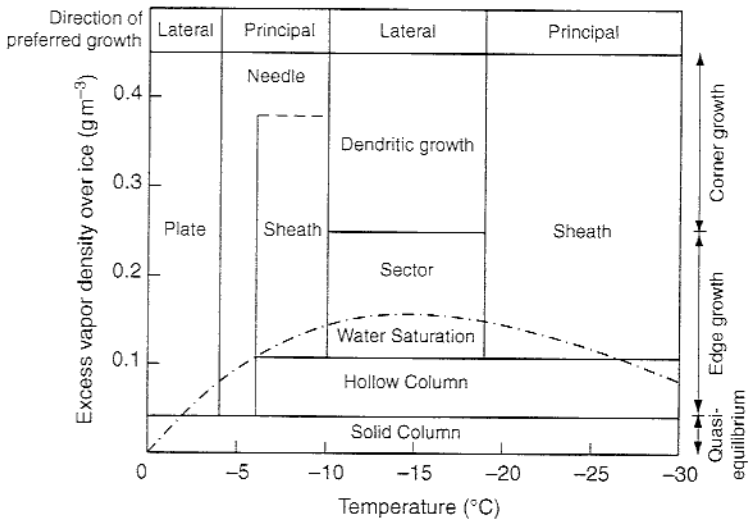

Figure 7.2. Diagram of ice crystal habit (form) as a function of temperature (°C) and excess vapor density above ice saturation over a flat ice surface as determined by measurements of T. Kobayashi. From Fletcher (1962). Bailey and Hallett (2004) provide an improved habit diagram for temperatures below −20 °C and extend the diagram to a temperature of −70 °C.

and higher, the hail stops as the hail shaft is exited. The temperature outside soon dips below freezing, and large snowflakes with the occasional raindrop are now seen. As the elevator continues upward, a wide variety of frozen particles (known as habits) are observed that look like needles, plates, snowflakes, and large clumped snowflakes (Fig. 7.2). This mixture of different particle shapes and sizes also contributes to the challenge of parameterizing microphysics, since these shapes and sizes influence how the particles interact with each other. Different vertical profiles of particles are seen in different parts of the thunderstorm, further complicating the situation. Yet parameterizations must be relatively simple if they are to be used in numerical models with predictive capabilities.

In this chapter a number of microphysics parameterizations are explored that typically are used for numerical model simulations with relatively small grid spacings. It is assumed in developing these schemes that there is no subgrid-scale variability in the microphysics variables within the model grid cells. However, this assumption cannot be used in climate models that use larger grid spacings and is an arguable assumption for many situations even for grid spacings below 30 km. Another approach is to allow for subgrid-scale variability in the microphysics parameterization by also calculating the fraction of the grid cell filled with cloud. In this way the grid cell is divided into

clear and cloudy portions. This type of approach typically uses a simpler microphysics parameterization combined with a diagnostic or predictive equation for cloud cover. As one might imagine, the specification of fractional cloud cover within a grid cell can lead to large changes in cloud–radiation interactions. Thus, an overview of microphysics parameterizations is presented in this chapter, and the additional complication of predicting cloud cover is saved for Chapter 9 in order to also include the effects of radiation in the discussion.

7.2 Particle types

Before examining the various microphysics parameterization schemes, it is important to overview briefly the physical processes that are important in the formation of the main microphysical particle types observed. These different hydrometeor types include cloud droplets, raindrops, ice crystals, aggregates, sleet, and rimed ice particles.

7.2.1 Cloud droplets

Liquid cloud droplets form when water saturation is exceeded over a range of temperatures from above freezing to about −40 °C. The Clausius–Clapeyron equation describes the equilibrium state for a system of water vapor over a flat liquid surface of pure water in which condensation and evaporation occur at identical rates. Since cloud droplets have a curved surface, an adjustment to the Clausius–Clapeyron equation is needed to account for the force of surface tension due to droplet curvature. This equation for the equilibrium vapor pressure (e_s) over the surface of a cloud droplet of radius r was derived by William Thomson, later Lord Kelvin, in 1870. It states that

$$e_s(r) = e_s(\infty)\, e^{2\sigma/rR_v\rho_w T}, \tag{7.1}$$

where σ is the surface tension (approximately 0.075 kg s^{-2} over the range of meteorologically relevant temperatures), ρ_w is the density of water, R_v is the gas constant for water vapor (461 J kg^{-1} K^{-1}), T is the temperature of the air, and $e_s(\infty)$ is the saturation vapor pressure over a flat liquid surface given by the Clausius–Clapeyron equation. This equation is often rearranged to express a saturation ratio S, such that

$$S = \frac{e_s(r)}{e_s(\infty)} = e^{2\sigma/rR_v\rho_w T}. \tag{7.2}$$

A saturation ratio with a value of 1 implies that the atmosphere is just saturated (i.e., the relative humidity equals 100%). Observed maximum saturation ratios in the atmosphere are typically less than 1.01, or 1% supersaturation. A numerical simulation by Clark (1973) suggests that supersaturations may reach 10% in localized regions of strong updrafts with precipitation, although these simulated high supersaturation values have yet to be verified or refuted by observations.

One would expect, and observations also indicate, that the first cloud droplets to form within a given air parcel are very small droplets. Yet the equilibrium vapor pressure $e_s(r)$ over a cloud droplet surface calculated using (7.1) increases as the droplet radius gets smaller. For typically initial cloud droplet radii, the required saturation ratio is above 2, or above 200% relative humidity! Since the maximum observed values of supersaturation in the atmosphere are much smaller, the formation of cloud droplets consisting of pure water is not common. The formation of cloud droplets instead depends most often on the presence of small particles in the atmosphere of micron size that have an affinity for water. Thus, it is not pure water that forms cloud droplets, but water in solution. The dissolved solute lowers the equilibrium vapor pressure. Thus, these particles, or aerosols, are centers for condensation and so are called cloud condensation nuclei (CCN). While the size and concentration of CCN vary across a large range, from 10^{-3} to 100 μm in size and orders of magnitude in concentration, they are very common in the atmosphere.

The presence of CCN necessitates a further modification to the equation for the saturation ratio. This leads to the expression (Rogers 1976)

$$S = \frac{e_s(r)}{e_s(\infty)} = \left(1 - \frac{b}{r^3}\right) e^{2\sigma/rR_v\rho_w T}, \tag{7.3}$$

where $b = 3im_S M_W/4\pi\rho_L M_S$, m_S is the solute mass (kg), M_S is the molecular weight of the solute, M_W is the molecular weight of a water molecule (18.016), and i is the degree of ionic dissociation (e.g., $i = 2$ for a dilute NaCl solution). For a given temperature T and solute type and mass, the resultant curve of saturation ratio S versus droplet radius r (called a Köhler curve) shows several interesting features (Fig. 7.3). First, for small radii, the solution effect dominates and for very tiny droplets the drop can be in equilibrium with the environment at values of S less than 1.0 (or relative humidities of less than 100%). This behavior (called deliquescence) accounts for haze in the atmosphere that restricts visibility and can turn the sky white instead of blue. For large radii, the surface tension effect dominates. In between these two extremes is where cloud droplet life is very interesting. When the slope of the curve is

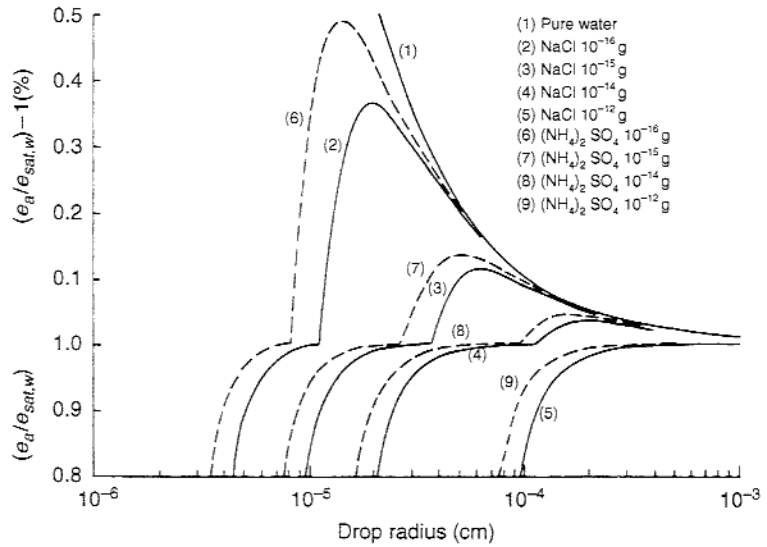

Figure 7.3. Equilibrium vapor pressure over an aqueous solution drop as a function of drop radius (cm) for various amounts of NaCl (solid lines) and $(NH_4)_2SO_4$ (dashed lines) in solution at 20 °C. From Pruppacher and Klett (2000).

positive, an increase in S is required for the drop to grow in size. However, once the slope equals zero, a critical point occurs. If the drop grows in size beyond where the slope is zero (the peak in the curve), it continues to grow without an increase in S and reaches cloud droplet sizes of at least 10 μm.

The radius at which the peak of the curve is reached is called the critical radius r^*. Drops with radii smaller than r^* only grow in response to increases in environmental relative humidity (or S), and therefore often are called haze particles. Also note that the greater the mass of the solute, the larger the value of r^* becomes. When a drop exceeds r^*, then the simple relationships discussed so far suggest that it grows indefinitely. However, in reality many water drops compete for the available water vapor and the environmental relative humidity decreases and not all drops continue to grow.

The initial growth of a cloud droplet is due to condensation and is proportional to $(S-1)/r$. Thus, as the droplet gets bigger its rate of growth slows. Because of this effect, the timescale required for condensation to produce raindrops is much longer than the timescale over which actual clouds produce precipitation. Another, more efficient mechanism for droplet growth must be acting, namely collision and coalescence, to greatly accelerate droplet growth. However, the collision and coalescence mechanism requires the presence of a

distribution of droplet sizes and fall speeds to be effective. At present it is uncertain exactly how the cloud droplet size spectrum is broadened sufficiently to allow for collision and coalescence to occur. It may be that the aerosol size distribution or cloud turbulence fills this role.

7.2.2 Raindrops

Once the cloud droplet size spectrum is sufficiently broad and some larger drops are present, droplets can grow by collisions and subsequent coalescences with other drops. This typically happens because of the differing fall velocities of the drops. For sea-level conditions, Gunn and Kinzer (1949) indicate that 0.1 mm diameter drops fall at 0.27 m s^{-1}, 1 mm drops fall at 4.03 m s^{-1}, 2 mm drops fall at 6.49 m s^{-1}, 4 mm drops fall at 8.83 m s^{-1}, and 5.8 mm drops fall at 9.17 m s^{-1}. These fall velocities increase as the pressure decreases. Thus, it is easy to imagine that collisions between drops can occur due to differences in fall velocities. Unfortunately, a droplet collision does not imply necessarily that the two droplets simply coalesce to form a single drop. Instead, a number of outcomes are possible. Some droplets collide and coalesce into a larger droplet. Other droplets collide and then bounce apart. Droplets also may collide and coalesce temporarily, and then separate into droplets similar to their initial pre-collision sizes or break into a number of smaller droplets. Large drops, in particular, tend to separate after collision to form two large drops and a number of smaller satellite drops.

The concept of efficiencies is used to define the likelihood that two drops actually collide and coalesce. The collision efficiency is the fraction of drops with radius r that collide with a larger drop of radius R as the larger drop overtakes the smaller drops (Figs. 7.4 and 7.5). The coalescence efficiency is then the fraction of drops that remain together after the collision. Finally, the collection efficiency is the collision efficiency multiplied by the coalescence efficiency. To obtain the total change in the size of the collector drop with initial radius R, it is necessary to integrate over all drop sizes less than or equal to R. In general, it is found that collection efficiencies for small drops are small and the efficiency increases with drop size up to drops with radius of around 1 mm. Above this point the collection efficiency depends upon the relative sizes of r and R. Small drops tend to move with the air flow around the larger drops and this leads to lower collection efficiencies when the difference in droplet size becomes large. This decrease in efficiency also happens when the droplets are similar in size.

Raindrops are limited in size owing to both collisions with other drops and the drops becoming unstable. As raindrops increase in size, they are less and

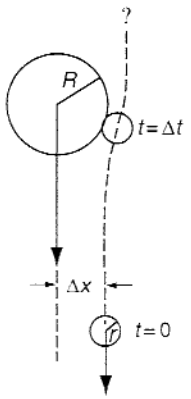

Figure 7.4. Schematic diagram depicting a large raindrop with radius R overtaking a smaller raindrop with radius r. The drops are separated at time $t=0$, but collide at time $t=\Delta t$ owing to the larger drop having a faster fall speed. The drops may or may not coalesce after collision. The centers of the drops are initially separated by distance Δx, but this changes as the drops get closer owing to the flow around the larger raindrop. After Rogers (1976).

less likely to permanently coalesce when they collide and instead may break upon collision into several smaller drops. In addition, aerodynamically induced circulations occur within the raindrop as it falls. For drop diameters above 3 mm the effects of surface tension are no longer certain to hold the drop together in the face of the drop rotational energy. Grazing collisions can produce a spinning drop that elongates and quickly breaks apart. The tendency for raindrops to break up as their diameters increase explains in part the negative exponential distribution of raindrops (Rogers 1976).

Rain can develop in a cloud within 15 min after cloud formation, although it may take longer before rain is observed at the ground. Since condensation alone is unable to produce large enough drops in such a short time period, collision and coalescence are the dominant mechanisms for producing raindrops so quickly. However, when the cloud becomes sufficiently deep, cold cloud precipitation processes occur and melting snow and graupel may provide most of the rain production.

When raindrops freeze, or when large melted snowflakes refreeze as they fall through a layer with temperatures below freezing near the ground surface, sleet or ice pellets may be produced. Sleet consists of small, generally transparent, solid grains of ice. Sleet that reaches the ground and freezing rain (rain that falls as liquid but freezes upon contact with the ground or other objects) are significant winter forecast concerns as they lead to very slick and dangerous surface conditions.

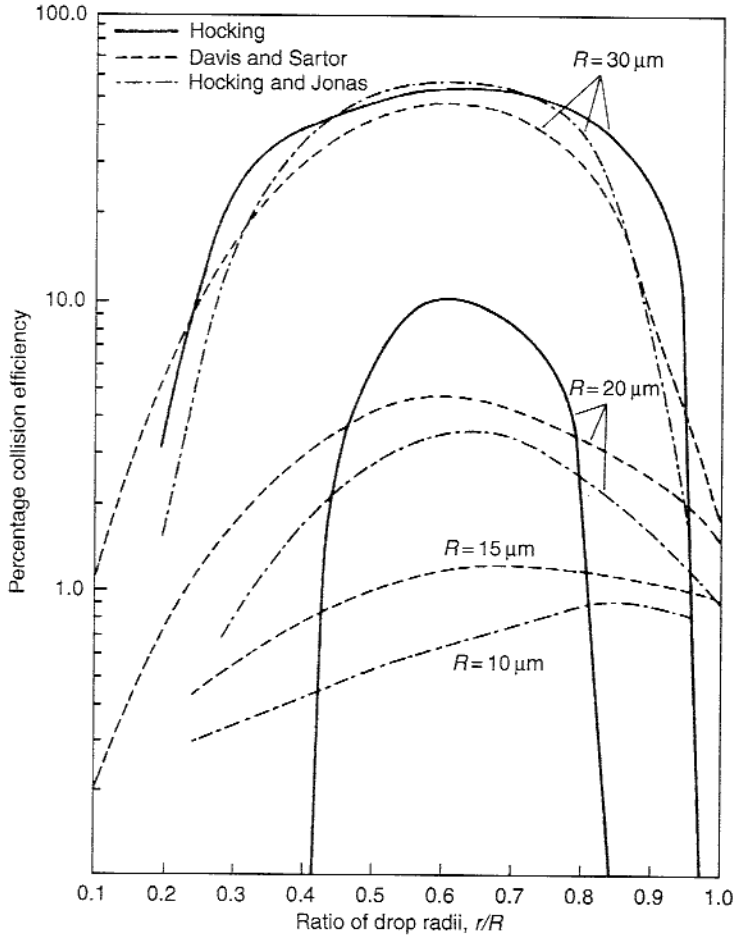

Figure 7.5. Collision efficiencies as a function of the raindrop size ratio (r/R) calculated by Hocking (1959), Davis and Sartor (1967), and Hocking and Jonas (1970). From Mason (1971).

7.2.3 Ice crystals and aggregates

When the temperatures within the cloud are below freezing, ice crystals may form. However, the freezing of cloud droplets may not occur immediately when the temperature drops below freezing and liquid drops have been observed down to temperatures near −40 °C. This unusual situation occurs because, unlike pools of water where a single ice nucleation event anywhere in the pool causes the entire pool to freeze, each individual cloud droplet must have an ice nucleation event. Evidence suggests that the homogeneous freezing of liquid drops happens when temperatures are below −40 °C.

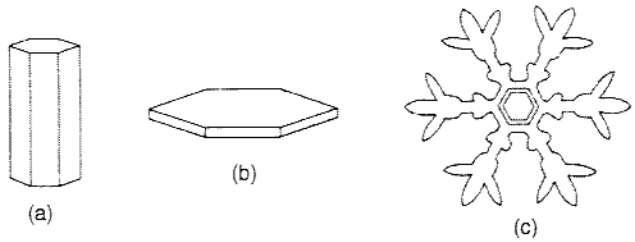

Figure 7.6. Sketches of the three habits of ice crystals: (a) column, (b) plate, and (c) dendrite. From Rogers (1976).

For temperatures warmer than −40 °C, the formation of ice requires the presence of an ice nucleus, just like CCN are needed for the formation of cloud drops. Four processes are believed to lead to ice nucleation: vapor-deposition nucleation, condensation-freezing nucleation, immersion-freezing nucleation, and contact-freezing nucleation. Vapor-deposition nucleation is the direct transfer of water vapor to an ice nucleus, resulting in the formation of an ice crystal. Condensation-freezing nucleation is the condensation of water onto an ice nucleus to create an embryonic drop, which is followed by the freezing of the embryonic drop. Immersion-freezing is the freezing of a supercooled liquid drop on an ice nucleus that is immersed within the liquid of the drop. Finally, contact-freezing nucleation is the freezing of a supercooled drop by an ice nucleus that comes into contact with the drop surface.

Ice crystals typically are observed starting at temperatures of −15 °C. There are three main forms, or habits, of ice crystals: columns, plates, and dendrites (Fig. 7.6). The habit of ice crystal growth is temperature, ice supersaturation, and initial nucleation process dependent (Bailey and Hallett 2004) and changes as the ice crystal moves through the cloud and experiences different environmental conditions. Note that larger drops tend to freeze at warmer temperatures.

The availability of ice nuclei (IN) also is temperature dependent. As the temperature decreases below 0 °C, more IN are available to help produce ice crystals. However, there remains a large discrepancy between the number of IN and the number of ice crystals observed, with more ice crystals being observed than would be expected based upon the observed number of IN. This discrepancy decreases with decreasing temperature, but can be as large as several orders of magnitude (10^4–10^5) in some cases (e.g., Hobbs and Rangno 1985).

Once ice crystals are produced, they can grow by vapor-deposition if the environment is supersaturated with respect to ice. Since saturation vapor pressure with respect to water is higher than saturation vapor pressure with respect to ice, any cloud that is saturated with respect to water is supersaturated

with respect to ice. Supersaturations of 10% or more with respect to ice are common. Thus, as ice crystals grow by vapor deposition they reduce the environmental supersaturation with respect to water until the air becomes subsaturated and liquid drops begin to evaporate. This evaporation then increases the supersaturation with respect to ice, and further encourages ice crystal growth. This process is called the Bergeron–Findeisen mechanism of ice crystal growth.

The processes of collision and coalescence can also produce clusters of ice crystals, called aggregates. Snowflakes are formed via this aggregation process. The collision and coalescence process for ice crystals is more complicated than for liquid drops owing to the various habits of the individual ice crystals and the possibility of mechanical interlocking or sticking after collision. In addition, whereas the coalescence efficiency for cloud drops is near unity, this is not necessarily the case for ice crystals. Laboratory experiments suggest that the coalescence efficiencies are higher at warmer temperatures ($>-5\,^{\circ}C$) and are a function of crystal habit. As aggregates fall through a cloud, typically at fallspeeds of less than $1\,m\,s^{-1}$, one can imagine them turning and changing velocity as different faces of the aggregates interact with the airflow. All this variability leads to uncertainty in how to describe the aggregation process in mathematical terms.

7.2.4 Rimed ice particles, graupel, and hail

Riming occurs as ice crystals collide and coalesce with supercooled cloud droplets at environmental temperatures below freezing (Fig. 7.7). When these collisions occur, the supercooled droplets freeze rapidly. As long as the features of the original ice particle can be distinguished, the ice particle is called a rimed particle. However, when the initial particle shape can no longer be distinguished, then the ice particle is typically considered a graupel particle. Graupel particles typically fall at speeds of $1–3\,m\,s^{-1}$ (Nakaya and Terada 1935), depending in part upon the density of the graupel particle. Graupel particle density varies across a large range owing to variations in the denseness of the frozen drops on the ice crystal. Graupel particles also serve as embryos for hailstones, which fall an order of magnitude faster at $10–50\,m\,s^{-1}$. A large fraction of convective rainfall is meltwater graupel in strong thunderstorms and thus is produced via cold cloud processes.

Graupel-sized particles are produced initially both by ice crystal riming and drop freezing. Of these two processes, ice crystal riming is by far the slowest since it takes time for small ice crystals to grow by vapor deposition and aggregation until they are large enough to have an appreciable fallspeed.

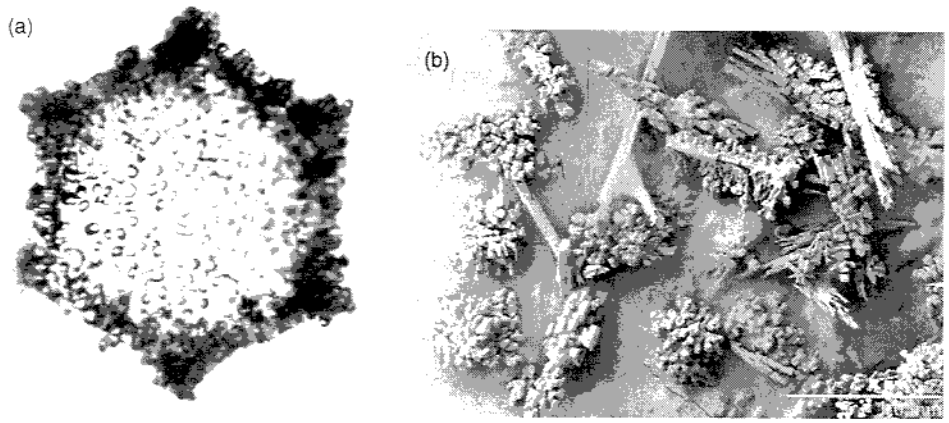

Figure 7.7. Picture of a rimed snowflake (left) and rimed column (right). From Hobbs *et al.* (1971) and the Electron Microscopy Unit of the Beltsville Agricultural Research Center of the United States Department of Agriculture, respectively.

Once they begin to fall, then riming can be very effective in growing the ice crystal into a graupel particle as supercooled cloud droplets are collected. In contrast, drop freezing by contact-freezing nucleation is a more rapid process of graupel generation. Small ice crystals collide with supercooled raindrops, leading to drop freezing and the instant formation of graupel-sized particles (Lamb 2001). A feedback mechanism may develop in which riming contributes both to the growth of graupel particles and to the production of secondary ice particles from splintering. These secondary ice particles grow by vapor deposition and add to the population of small ice particles that can lead to contact-freezing nucleation (Hallett and Mossop 1974). However, this process is not active in all clouds.

As graupel particles fall through the liquid cloud they continue to grow via riming. In cases of extreme riming, hailstones are formed. Hailstones are typically several centimeters in diameter, but observations indicate that hailstones as large as 10–15 cm can occur (Knight and Knight 2005). The latent heat of fusion from freezing accreted droplets heats the surface of the stone, thus slowing the rate of droplet freezing and influencing the growth of the hailstone. Owing to this latent heat release, a growing hailstone is often several degrees warmer than its environment. When the hailstone temperature remains below freezing, "dry" growth occurs as all collected droplets freeze upon contact. When the hailstone temperature rises to 0 °C, "wet" growth occurs as the collected droplets no longer freeze on contact. Instead, some of the collected water from the droplets is frozen, while the remaining unfrozen water is either lost by shedding or incorporated into the hailstone to form spongy ice. The liquid fraction of large hailstones may exceed 20%. During the

lifetime of a hailstone, periods of both dry and wet growth may occur, thereby developing the layered onion-like structure observed in hailstone cross-sections (Rogers 1976; Ziegler *et al.* 1983).

7.3 Particle size distributions

When sampling all the liquid or ice particles within a specified volume of air, observations show a distribution of particle sizes. These distributions specify the number of particles per unit size interval (typically the particle diameter) per unit volume of air. All measurements indicate a rapid decrease in the number of particles as the particle size increases. Also seen is a tendency for an increasing number of larger particles as the precipitation intensity increases.

A function that approximates the distribution of particles well is an inverse exponential function, first suggested by Marshall and Palmer (1948). Thus, particle distributions can be approximated by

$$n(D) = n_0 e^{-\lambda D}, \tag{7.4}$$

where D is the particle diameter (m), n is the number of particles per unit volume (m^{-4}), λ is the slope parameter that defines the fall off of particles as the diameter increases (m^{-1}), and n_0 is the intercept parameter that defines the maximum number of particles per unit volume at $D = 0$ size.

While observations of particle distributions typically depart from the pure negative exponential, this simple expression tends to be the limiting form when samples of the distributions are averaged (Fig. 7.8). This is true for raindrops, snow crystals, graupel, and hail. Thus, the Marshall–Palmer distribution is a common assumption in many parameterizations of cloud microphysical processes. The gamma distribution also is used to describe particle distributions, varing from the inverse exponential distribution mainly for very small droplet sizes. Smith (2003) argues that the observational limitations at very small droplet size produce larger uncertainties in the particle distributions than the differences in the bulk properties between the gamma and inverse exponential distributions.

For those interested in pursuing the details of cloud physics, the books by Rogers (1976), Cotton and Anthes (1989), Rogers and Yau (1989), Houze (1993), Pruppacher and Klett (2000), are wonderful resources. For present interests, suffice it to say that the microphysical processes are complex, require approximations for numerous interactions, and are founded upon a less than perfect observational and theoretical base. Yet this understanding is sufficient to begin the parameterization process with some hope of success.

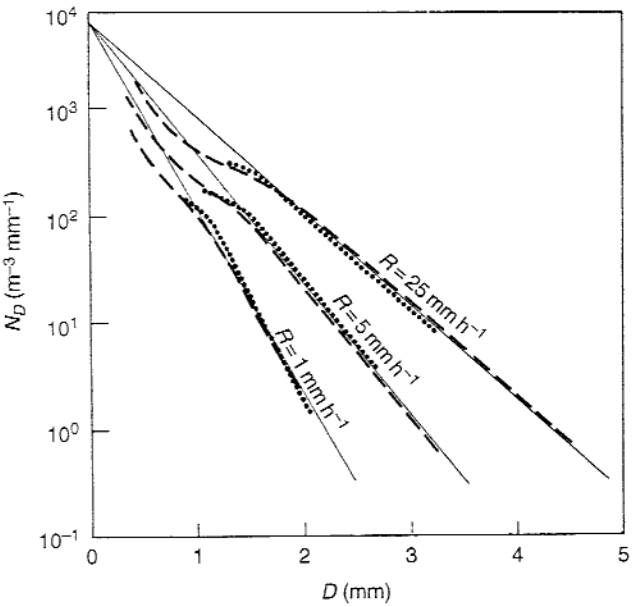

Figure 7.8. Observed drop-size distributions (dots) for different rain rates (R in mm h^{-1}) compared with best-fit inverse exponential curves (solid lines) and drop distributions reported by others (dashed lines). From Marshall and Palmer (1948).

7.4 Bulk microphysical parameterizations

Microphysical parameterizations typically are grouped into "bulk" and "bin" approaches. Bulk approaches use a specified functional form for the particle size distributions and generally predict the particle mixing ratio (total mass per unit volume of air), although some bulk approaches can, in addition, predict the total particle concentration (Ziegler 1985; Ferrier 1994; Meyers *et al.* 1997). Schemes that predict only the particle mixing ratio are called single-moment schemes, while those that predict the particle mixing ratio and concentration are called double-moment schemes. Triple-moment schemes are available, but are used in only a very few research models (e.g., Clark 1974). Often the particle size distribution is approximated by the inverse exponential distribution in bulk approaches, although gamma functions and log-normal functions also have been used to describe some hydrometeor distributions (e.g., Clark 1976; Ziegler 1985; Ferrier 1994). In contrast, a bin approach does not use a specified function for the particle distribution, and instead divides the particle distribution into a number of finite size or mass categories (Berry 1967; Kogan 1991; Ovtchinnikov and Kogan 2000; Lynn *et al.* 2005). This division of the

particle distribution into numerous bins requires much larger memory and computational capabilities, and poor knowledge of ice phase physics hampers the accurate representation of evolving ice particle concentrations. Therefore, bin models are employed in only a few research models and presently are not used in operational models. Thus, bulk microphysical parameterizations are the focus of this chapter.

One benefit to using double-moment schemes that predict both the particle mixing ratio and the concentration, in comparison to single-moment schemes that predict only the particle mixing ratio, is that double-moment schemes should be applicable across a wider range of environments. McCumber *et al.* (1991) suggest that different single-moment parameterizations must be used to simulate correctly the hydrometeor structure of organized convective systems in different large-scale environments, since these systems often have two or more regions with vastly different hydrometeor number concentrations. Since double-moment schemes should require less tuning of parameters that are related to particle number concentrations (e.g., Ferrier *et al.* 1995), they should perform better over a larger range of environmental conditions. Similarly, the benefits of using a bin approach in comparison to a bulk approach are that the scheme includes more specific parameterizations of various microphysical processes and the interactions between particles. However, these schemes also are more computationally expensive as they require a larger number of calculations.

One common and important assumption in many of the schemes examined is that cloud water and the smallest cloud ice particles are monodisperse and do not move relative to the flow, so they are simply advected with the flow both horizontally and vertically (see Fig. 7.9). Precipitating particles (raindrops, snow, graupel, and hail), on the other hand, have significant fall speeds and move relative to the flow. This clean separation in drop size between cloud water and rainwater, for example, is seen in numerical simulations of cloud droplet growth and precipitation development after collision and coalescence acts over time to broaden the drop size distribution (Fig. 7.10; Berry 1965; Cotton 1972; Berry and Reinhardt 1974a).

Another important assumption is the type of function used to approximate the distribution of particles within a volume. Many schemes assume a Marshall–Palmer-type inverse exponential distribution in which the intercept parameter n_{0x} is specified and assumed to be constant throughout the simulation. Thus, the slope parameter λ_x varies as the mixing ratios change, where

$$\lambda_x = \left(\frac{\pi \rho_x n_{0x}}{\rho q_x} \right)^{1/4}. \tag{7.5}$$

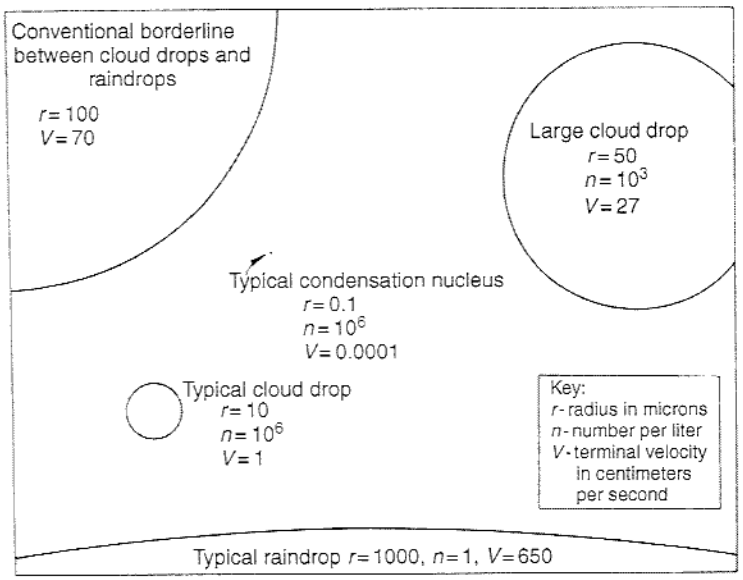

Figure 7.9. Schematic diagram of the relative sizes, concentrations, and fall velocities of some of the particles involved in warm cloud processes. From McDonald (1958), reprinted with permission from Elsevier.

Here x refers to the particle type ($x = r$, s, g for rain, snow, or graupel, respectively), ρ_x is the density of the particle, ρ is the atmospheric density, and q_x is the mixing ratio. Other choices for the function used to define the distributions are gamma functions (e.g., Ziegler 1985; Ferrier 1994). It is often helpful to note that the value of λ_x^{-1} yields the mean particle diameter. In double-moment schemes, the constant n_{0x} is replaced by the variable n_x.

The various bulk microphysical parameterization schemes in the literature can vary in both the approximations used to describe the interplay between the different particles and the number of interactions (both phase and habit changes) included in the parameterization scheme. For example, the Dudhia (1989) simple ice scheme incorporates 12 different interactions between water vapor, cloud water, rainwater, ice, and snow. The Lin *et al.* (1983) and Reisner *et al.* (1998) schemes both include 32 different interactions between water vapor, cloud water, rainwater, ice, snow, and graupel. While most of the bulk microphysical schemes in use today include both water and ice processes, there remain some schemes or models that only include warm phase microphysics (i.e., cloud water and rainwater only). Johnson *et al.* (1993) and Gilmore *et al.* (2004a) indicate that differences in both the amount of rainfall and the cold pool strength occur when ice processes are included in model simulations of

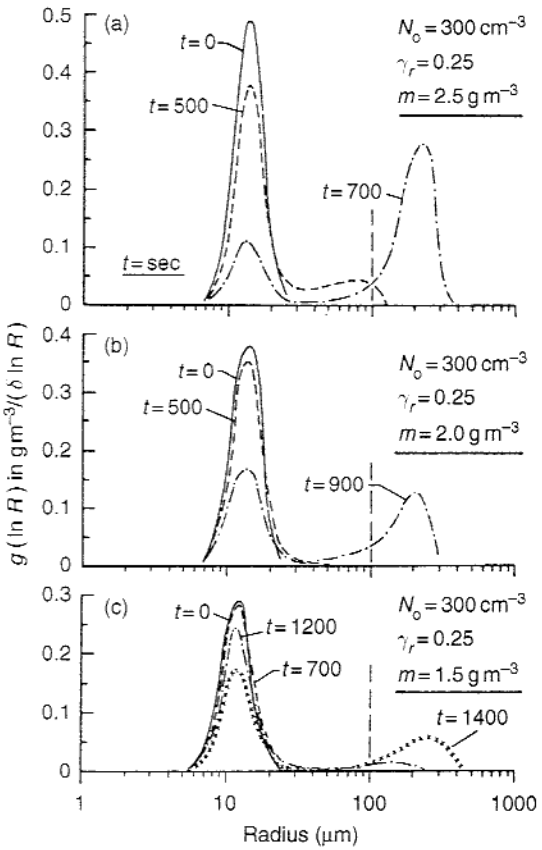

Figure 7.10. Computed distributions of the water mass density at various times between initial time ($t = 0$) and 1400 s (indicated on each panel) for an initial cloud droplet concentration of 100 cm^{-3}, a radius of dispersion of 0.25, and liquid water contents of 2.5 (top), 2.0 (middle), and 1.5 (bottom) g m^{-3}. The Kessler (1969) threshold radius separating cloud droplets from raindrops is shown by the vertical dashed line. Note the fairly distinct separation of sizes between cloud drops and raindrops, with few drops being in between the two distributions. From Cotton (1972).

thunderstorms as compared to simulations with only warm-phase microphysics. Thus, it remains important to understand the details in the schemes that one uses to forecast or simulate atmospheric processes.

The equations that govern the evolution of the microphysical variables all follow a similar structure, namely

$$\frac{\partial q_x}{\partial t} = -ADV(q_x) + TURB(q_x) + (P_1 + P_2 + P_3 + P_4 + P_5 + \cdots), \quad (7.6)$$

where q_x is any microphysical variable (e.g., mixing ratios of water vapor, cloud water, rainwater, ice, snow, and graupel), ADV represents the advective processes, $TURB$ represents the turbulent processes, and P_i represents the various tendencies from the microphysics parameterization. These tendencies can be either a positive or a negative contribution to the total tendency for q_x. For example, condensation produces a positive cloud water tendency, whereas evaporation produces a negative cloud water tendency. In addition, the tendencies in the microphysical variables often involve latent heat release, and so their effects also must be incorporated into the temperature tendency equation. Thus, while this chapter examines how the various microphysical interaction terms are parameterized, the connections to the other model variables (temperature, water vapor mixing ratio) also need to be made even if they are not discussed specifically.

Perhaps the best approach to understanding how these bulk microphysical schemes operate is to explore in detail how some of the particle interaction approximations are derived. There are a large number of microphysical parameterizations in the literature, and it is impossible to discuss them all. Instead, the approach taken here is to take an overview of the general ideas and some similarities between a handful of commonly used schemes to provide the reader with a basic understanding of how the broader class of schemes operate. We begin with the process of condensation.

7.4.1 Condensation

Most single-moment bulk microphysical schemes parameterize condensation following Asai (1965), and the following largely follows this discussion. The tendency for producing supersaturation in the atmosphere is nearly completely offset by the condensation of many tiny cloud drops. Thus, when water vapor condenses and cloud droplets are formed, we have the supersaturation condition that

$$q_v - q_{vs} = \delta M > 0, \tag{7.7}$$

where q_v is the water vapor mixing ratio ($\mathrm{kg\,kg^{-1}}$), q_{vs} is the saturation water vapor mixing ratio ($\mathrm{kg\,kg^{-1}}$), and δM represents the total possible condensed water ($\mathrm{kg\,kg^{-1}}$). However, in actuality, δM is divided into two parts ($\delta M = \delta M_1 + \delta M_2$): condensed water δM_1 (cloud water) and an increase in the water vapor mixing ratio to be stored in the air δM_2, owing to the latent heat release from condensation that produces a warmer air temperature and a greater saturation water vapor mixing ratio.

The warming due to condensation can be expressed as

$$\delta\theta_1 = \frac{L_v}{c_p}\left(\frac{p_0}{p}\right)^{\kappa}\delta M_1, \tag{7.8}$$

where L_v is the latent heat of vaporization, c_p is the specific heat at constant pressure, p_0 is the surface pressure (Pa), p is the pressure (Pa), and $\kappa = R_d/c_p = 0.286$. Now, the Clausius Clapeyron equation states that

$$\frac{de_s}{dT} = \frac{L_v e_s}{R_v T^2}. \tag{7.9}$$

where e_s is the saturation vapor pressure (Pa), R_v is the individual gas constant for water vapor (461 J kg^{-1} K^{-1}), and T is temperature (K). One can replace the vapor pressure by a mixing ratio using the approximation

$$e = \frac{q_v p}{\varepsilon}, \tag{7.10}$$

which leads to a modified version of the Clausius–Clapeyron equation

$$d\left(\frac{q_{vs}p}{\varepsilon}\right) = \frac{L_v(q_{vs}p/\varepsilon)}{R_v T^2}\, dT. \tag{7.11}$$

If the pressure is assumed to be constant, then this equation simplifies to

$$dq_{vs} = \frac{L_v q_{vs}}{R_v T^2}\, dT. \tag{7.12}$$

From the definition of potential temperature, we have

$$T = \theta\left(\frac{p}{p_0}\right)^{\kappa}. \tag{7.13}$$

Thus, the dT in the modified Clausius Clapeyron equation can be replaced by $d\theta$, such that

$$dq_{vs} = \frac{L_v q_{vs}}{R_v \theta^2}\left(\frac{p_0}{p}\right)^{\kappa} d\theta. \tag{7.14}$$

Finally, replace $d\theta$ with $\delta\theta_1$ to represent the warming effect of condensation, and dq_{vs} with δM_2 to represent the increased saturation mixing ratio due to warming. This leads to

$$\delta M_2 = \frac{L_v^2}{c_p R_v}\left(\frac{p_0}{p}\right)^{2\kappa}\frac{q_{vs}}{\theta^2}\,\delta M_1. \tag{7.15}$$

and so the ratio of $\delta M_1/\delta M$ is

$$\frac{\delta M_1}{\delta M} = r_1 = \frac{1}{\left[1 + \left(L_v^2/c_p R_v\right)(p_0/p)^{2\kappa}\left(q_{vs}/\theta^2\right)\right]}. \tag{7.16}$$

Thus, the increase in cloud water over the model time step (Δt) due to condensation (P_{COND}) is

$$P_{COND} = (r_1\ \delta M)/\Delta t. \tag{7.17}$$

Over the same time interval, the value of q_v must then decrease by the same amount, so that the air is just saturated when the latent heating from condensation is included in the temperature tendency equation. This approach is used within the schemes of Rutledge and Hobbs (1983), Dudhia (1989), and Reisner *et al.* (1998). A similar adjustment approach for the condensation tendency term is used by Tripoli and Cotton (1980) and Schultz (1995), although the adjustment factor used by Schultz is constant ($r_1 = 0.75$) and does not vary with the environmental conditions. Asai (1965) indicates that r_1 varies from 0.25 to 0.9 for a lapse rate of 6.5 °C km^{-1} and temperatures between freezing and 30 °C. If the supersaturation of the environment is less than 1, then evaporation occurs using the same parameterization but with the sign reversed.

Now that cloud droplets can form in the model, we look to see how rain water is created. As discussed earlier, rain is first formed from the cloud droplets through a binary collision–coalescence process called "autoconversion."

7.4.2 Autoconversion

Autoconversion is the process where cloud droplets collide and coalesce with each other and eventually form raindrops. Many parameterizations follow Kessler (1969) in specifying a relationship that resembles

$$P_{AUTO} = \max[k_1(q_c - q_{c\_threshold}), 0], \tag{7.18}$$

where q_c is the cloud water mixing ratio (kg kg^{-1}), k_1 is a conversion rate, and $q_{c\_threshold}$ is a threshold value for q_c (kg kg^{-1}) below which autoconversion does not occur. Dudhia (1989) and Reisner *et al.* (1998) both use $k_1 = 0.001$ s^{-1} and $q_{c\_threshold} = 0.0005$ kg kg^{-1}.

Lin *et al.* (1983) use a slightly different expression for autoconversion that is based upon the relation suggested by Berry (1968). Gilmore *et al.* (2004b) rederive the Lin *et al.* (1983) microphysics scheme, providing additional detail. Instead of a linear relationship between the autoconversion rate and q_c, Lin *et al.* (1983) suggest a quadratic relationship such that

$$P_{AUTO} = \frac{1 \times 10^{-3}[\rho(q_c - q_{c\_threshold})^2]}{\{1.2 \times 10^{-4} + [1.569 \times 10^{-18} N_1 / D_0 \rho(q_c - q_{c\_threshold})]\}}, \quad (7.19)$$

where N_1 is the number concentration of cloud droplets ($1 \times 10^9\,\mathrm{m}^{-3}$) and D_0 is the dispersion of the cloud droplet distribution and is assumed to be 0.15. The threshold value for the cloud water mixing ratio is set to $0.002\,\mathrm{kg\,kg}^{-1}$ in Lin *et al.* (1983), a value four times larger than that of Dudhia (1989) or Reisner *et al.* (1998). A similar approach is used by Ferrier (1994), except that the autoconversion threshold is a function of the droplet number concentration.

Another parameterization for autoconversion is proposed by Tripoli and Cotton (1980). This approach again uses a threshold value for q_c below which there is no conversion. However, they also include a factor that represents the mean collision frequency for cloud drops that become raindrops after colliding. This leads to the expression

$$P_{AUTO} = \frac{0.104 g E \rho_0^{4/3}}{\mu (n_c \rho_w)^{1/3}} q_c^{7/3} h(q_c - q_{c\_threshold}), \quad (7.20)$$

where the collection efficiency $E = 0.55$, the mean cloud droplet concentration $n_c = 3 \times 10^8\,\mathrm{m}^{-3}$, the cloud water mixing ratio threshold $q_{c\_threshold} = 0.0005\,\mathrm{kg\,kg}^{-1}$, ρ_0 is the density of the hydrostatic reference state, and μ is the dynamic viscosity

$$\mu = 1.72 \times 10^{-5}[393/(T + 120)](T/273)^{3/2}, \quad (7.21)$$

where T is in kelvin and μ has units of $\mathrm{kg\,m}^{-1}\,\mathrm{s}^{-1}$. The Heaviside stepfunction $h(x)$ equals 0 when $x < 0$, equals 0.5 for $x = 0$, and equals 1 for $x > 0$. This initially produces a more gradual conversion rate than compared to the Kessler approach, but produces a larger conversion rate at high cloud water mixing ratios. The autoconversion parameterization of Berry and Reinhardt (1974b) as adapted by Walko *et al.* (1995) also tends to produce lower conversion rates than the Kessler approach (Thompson *et al.* 2004).

Cotton and Anthes (1989) indicate that the conversion rates from several parameterizations of autoconversion differ by several orders of magnitude. Since the rain formation process is dominated by accretion, the collection of cloud droplets by raindrops, the magnitude of the autocollection rate may not be important. However, Cotton (1972) and Cotton and Anthes (1989) also mention that it takes time for cloud droplets to transform into raindrops. This "aging" period is not included in any of these parameterization schemes, and may lead to the early production of rain water too low in the cloud (Simpson

and Wiggert 1969; Cotton 1972). Straka and Rasmussen (1997) suggest incorporating a separate tendency equation for the age of a process or the condition of parcels (in a Lagrangian sense) that could be used to delay the autoconversion process in Eulerian models and may yield better results. Using a double-moment scheme, Ziegler (1985) explicitly accounts for non-linear coalescence rates and finds the timing of rain formation to be reasonable.

In a similar manner, Schultz (1995) defines

$$P_{AUTO} = (l_c - l_{c\_threshold}), \tag{7.22}$$

where l_c is the specific content ($\mathrm{kg\,m^{-3}}$) of the cloud water and $l_{c\_threshold} \sim 0.0007\,\mathrm{kg\,m^{-3}}$. The specific content is related to the mixing ratio by a density scaling, where $l_c = \rho q_c$. Schultz uses specific contents instead of mixing ratios for processes that are independent of the air density, such as collection and diffusion. In the autoconversion approximation, the conversion only occurs if the rain water specific content l_r is zero – otherwise it is not allowed. Thus, Schultz is assuming that autoconversion may be important for the initial creation of raindrops, but not afterwards. Lin *et al.* (1983) suggest that their high plains thunderstorm simulation is more realistic when the autoconversion term is turned off, perhaps owing to the increased importance of cold cloud processes in these high-based thunderstorms.

7.4.3 Accretion

Accretion is the process by which a liquid drop collides and coalesces with smaller liquid drops as it falls. Kessler (1969) assumes that a raindrop falling through a layer of cloud droplets sweeps out a cylindrical volume as it falls, thereby having a chance to collect all the cloud droplets in its path. Thus, he defines the rate of rain mass accumulation due to the accretion of cloud droplets from a single raindrop as

$$\frac{d(m(D))}{dt} = \frac{\pi D^2}{4} E V_r \rho q_c, \tag{7.23}$$

where $m(D)$ is the mass of a raindrop of diameter D, E is the collection efficiency, V_r is the raindrop fall speed ($\mathrm{m\,s^{-1}}$ and assumed to be positive), ρ is the atmospheric density, and q_c is the cloud water mixing ratio. For $E = 1$, the raindrop accumulates all the cloud droplets in its path.

Equation (7.23) is a continuous growth equation, since for every time step there is a change in the mass of the droplet. However, as discussed by Telford (1955), the increase in droplet mass actually is a discrete process related to the specific number of cloud droplets collected. Telford (1955) takes into account

the discrete nature of the accretion process and develops a stochastic coalescence equation. The incorporation of the discrete nature of coalescence can lead to the development of a complete raindrop spectrum much faster than using the continuous growth assumption (Telford 1955). Ziegler (1985) develops a bulk parameterization based upon the stochastic coalescence equation.

To convert (7.23) to a bulk parameterization, integrate (7.23) over all raindrop sizes assuming a distribution for the raindrops. In many parameterizations, cloud drops are assumed to be monodispersed (all drops in the distribution are set to the same size, although the size can vary based upon the mixing ratio). This is one of the parameterizations for which the function used to define the distribution of particles is important. Kessler (1969), and many others, assume a Marshall–Palmer-type inverse exponential distribution, which then leads to the bulk expression for accretion. Thus, the rate at which the inverse exponential raindrop distribution accretes the monodispersed cloud droplet distribution is given by

$$P_{ACCR} \equiv \int_0^\infty \frac{d(m(D))}{dt} n(D)\, dD = \int_0^\infty \frac{\pi D^2}{4} E V_r \rho q_c n_{0r} e^{-\lambda D}\, dD, \tag{7.24}$$

where n_{0r} is the intercept parameter for the raindrop distribution and λ is the slope of the raindrop distribution. If one assumes $V_r = aD^b$, then with knowledge of the gamma function Γ we obtain

$$P_{ACCR} = \frac{\pi E}{4} \rho q_c n_{0r} a \frac{\Gamma(3+b)}{\lambda_r^{3+b}}. \tag{7.25}$$

The parameterizations of Lin *et al.* (1983), Dudhia (1989), and Reisner *et al.* (1998) are all based upon this derivation, and differ only in how they include corrections to the accretion rate as a function of height or pressure. Liu and Orville (1969) conduct a least-squares analysis of the fall speed data of Gunn and Kinzer (1949) and find that the constants a and b are 841.996 $\mathrm{m}^{1-b}\,\mathrm{s}^{-1}$ and 0.8, respectively (Gilmore *et al.* 2004b). However, raindrop fall speeds also vary with pressure, becoming larger as pressure decreases.

In contrast, Tripoli and Cotton (1980) re-express the inverse exponential raindrop distribution (7.5) as a function of the characteristic raindrop radius, yielding a constant value for λ and an intercept parameter n_{0r} that varies with rainwater content (see Fig. 7.11). Under this assumption, the terminal velocity of rain is independent of the rain density. They conclude that the accretion rate is

$$P_{ACCR} = 0.884 E \left(\frac{g\rho_0}{\rho_w R_m} \right)^{1/2} q_c q_r. \tag{7.26}$$

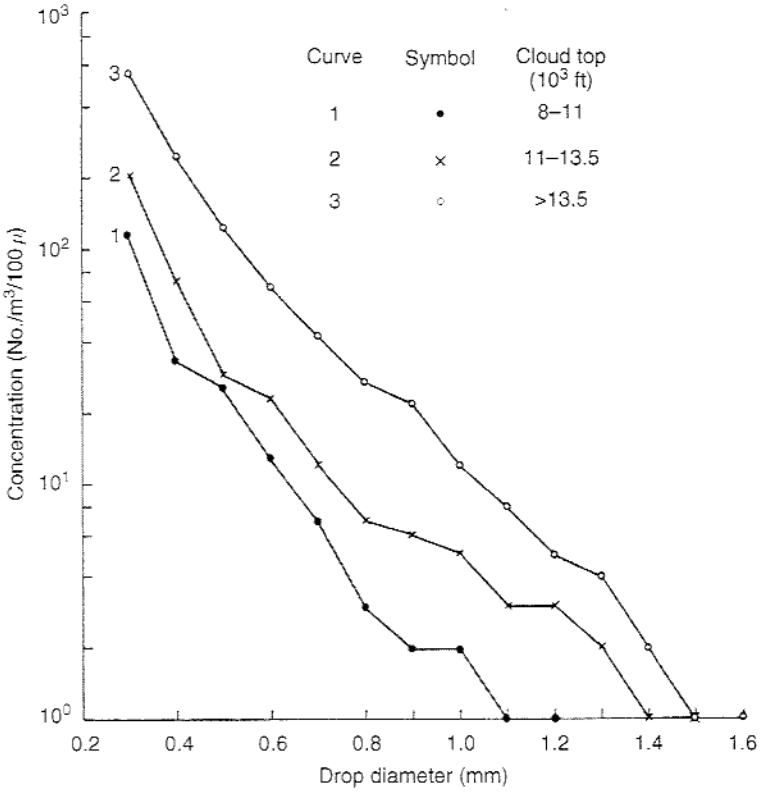

Figure 7.11. Mean drop size distributions in warm cumuli over southeast Texas where drop diameters must be >250 μm. Data are categorized according to estimated cloud tops (shown in 10^3 ft). Note how the distribution slope appears nearly constant, while the intercept parameter changes for the data associated with different cloud tops. From Klazura (1971).

where R_m is a characteristic drop radius taken as 2.7×10^{-4} m in Tripoli and Cotton (1980). This yields a lower accretion rate than Kessler with $E = 1.0$ when the water mass density is less than 2.28×10^{-3} kg m^{-3}. But the differences are small for higher water mass densities. They also define a variable E based upon the work of Langmuir (1948) in which

$$E = \begin{cases} 0 & \text{for } STK < 0.0833 \\ \dfrac{STK^2}{(STK + 0.5)^2} & \text{for } STK \geq 0.0833 \end{cases} \tag{7.27}$$

where STK is the Stokes number and

$$STK = \frac{0.22 \rho_w V_r(R_m) q_c^{2/3}}{R_m \mu} \left(\frac{0.239}{n_c/3} \right)^{2/3}. \tag{7.28}$$

Here ρ_w is the density of water and n_c is the mean cloud drop concentration (assumed to be $3 \times 10^8\,\mathrm{m}^{-3}$). The value of E calculated using (7.27) is greater than 0.95 for cloud water mixing ratios greater than $5.3 \times 10^{-7}\,\mathrm{kg\,kg}^{-1}$ and so is generally at or near 1.

Perhaps the simplest expression for accretion is given by Schultz (1995), where he defines

$$P_{ACCR} = 17 l_r l_c. \tag{7.29}$$

Again, the rate equations in Schultz are for specific content instead of the mixing ratio. The general idea is that the accretion rate depends upon both the rain water and cloud water specific contents, similar to Tripoli and Cotton (1980) except using mixing ratios. Note that the accretion rates of Lin *et al.* (1983), Dudhia (1989), and Reisner *et al.* (1998) are also dependent upon these two mixing ratios (q_r and q_c), but that the rain water mixing ratio is hidden in the definition of λ_r in (7.5). If this is made more explicit by combining (7.5) with (7.25), then the accretion rate depends upon $q_c q_r^{0.95}$, and so is not dramatically different from these other two expressions.

Cotton and Anthes (1989) indicate that even if one is comfortable with the function assumed for the raindrop distribution, it is likely that the distribution slope and intercept parameter vary independently throughout the lifetime of a cloud. Since one or the other is specified to be a constant in these bulk schemes, errors are likely. They argue that this is especially true for mesoscale convective systems that have both a convective line and a distinct trailing or forward stratiform precipitation region. The stratiform portion of the convective system is likely to have a different microphysical structure and history, and so any raindrop distributions assumed for the convective line may not be realistic for the stratiform region and vice versa. Differences in raindrop distributions between stratiform and convective regions of tropical mesoscale convective systems are seen from observations (Tokay and Short 1996). This observed horizontal and temporal variability in the microphysical parameters is certainly one challenge to these types of schemes.

7.4.4 Evaporation

Byers (1965) develops an equation governing the evaporation/condensation of a single raindrop. Both the effects of the vapor pressure difference between the drop and the ambient environment and the latent heat flux are taken into account. It is shown that

$$\frac{dm(D)}{dt} = \frac{2\pi D(S-1)}{A+B}, \tag{7.30}$$

where S is the supersaturation, and

$$A = \frac{L_v^2}{K_a R_v T^2}, \qquad B = \frac{R_v T}{e_S(T) D_{diff}}. \tag{7.31}$$

Here D_{diff} is the diffusivity of water vapor in air and K_a is the thermal conductivity. However, an additional effect is due to the ventilation of the drop as it falls and this effect also should be incorporated. Byers uses the results of Kinzer and Gunn (1951) to account for the ventilation, while others may use the results of Beard and Pruppacher (1971). Thus, the resulting equation for the evaporation of a raindrop that includes a ventilation factor F becomes

$$\frac{dm(D)}{dt} = \frac{2\pi D(S-1)F}{A+B}. \tag{7.32}$$

The ventilation factor F is often defined based upon the Schmidt number (S_c) and the Reynolds number (Re), such that

$$F = 0.78 + 0.31 S_c^{1/3} Re^{1/2}. \tag{7.33}$$

The Schmidt number is the ratio of kinetic viscosity to the diffusivity of water vapor and represents the relative ease of molecular momentum and mass transfer, while the Reynolds number is the ratio of inertial to viscous forces and indicates whether the flow is turbulent or laminar. Again, the total evaporation from all drops is then found by multiplying the equation for the evaporation of a single raindrop by the function that describes the raindrop distribution, and then integrating over all drop sizes. This approach is the basis for most of the evaporation expressions in various bulk microphysics schemes. The resulting equation typically resembles the following one taken from Lin *et al.* (1983), with

$$P_{EVAP} = \frac{2\pi(S-1)n_{0r}}{\left[\rho\left(\dfrac{L_v^2}{K_a R_v T^2} + \dfrac{1}{\rho q_{vs}\psi}\right)\right]} \times \left[0.78\lambda^{-2} + 0.31 S_c^{1/3}\Gamma\left(\frac{b+5}{2}\right) a^{1/2}\nu^{-1/2}\left(\frac{\rho_0}{\rho}\right)^{1/4}\lambda_r^{-(b+5)/2}\right], \tag{7.34}$$

where most of the variables are as previously defined, a and b are from the expression of fall velocity ($V_r = aD^b$), ν is the kinematic viscosity of air, and ψ is the diffusivity of water vapor in air.

Owing to their different assumptions, Tripoli and Cotton (1980) and Schultz (1995) have different expressions for evaporation. The different behavior of the raindrop distribution assumed in Tripoli and Cotton leads to a slightly different equation, but the evaporation rate is still a function of $(S-1)q_r$ and is still based upon the results of Byers (1965). In contrast, Schultz (1995) again simplifies the process to a rate equation directly related to $(S-1)$, but with the evaporation allowed in a given time step limited to a specified amount.

For warm rain processes only, the parameterizations for condensation, autocollection, accretion, and evaporation are the foundation of what is needed in a numerical model. Added to this is the assumed raindrop distribution functional, and the only remaining item of importance is the mass-weighted fall speed. All precipitating fields are assumed to fall at their mass-weighted fall speed, defined as

$$\overline{V}_r = \frac{\int_0^\infty n_r(D) m(D) V_r(D)\, dD}{\int_0^\infty n_r(D) m(D)\, dD}. \tag{7.35}$$

If we assume that raindrops are spheres, then the mass of a raindrop is $\pi D^3 \rho_w / 6$. We again assume that the fall speed of an individual raindrop can be approximated as $V_r = aD^b$, and that the raindrop distribution is represented by an inverse exponential, leading to

$$\overline{V}_r = \frac{a\Gamma(4+b)}{6\lambda_r^b}. \tag{7.36}$$

Expressions for the mass-weighted fall speed of rain differ based upon the approximations used for defining the constants a and b for the fall speed of an individual raindrop, and whether or not they add a density correction factor.

7.4.5 Ice initiation

The basic idea behind many parameterizations of ice initiation is that ice nuclei are activated to form ice crystals in ice supersaturated conditions, since the observed concentrations of ice nuclei appear to be sufficient to explain ice crystal concentrations in some atmospheric clouds. Thus, from predicted or known ice nucleus concentrations it is possible to calculate the concentration of vapor-activated ice crystals. Given the ice crystal concentration, knowledge of the mass of a typical ice crystal is sufficient to calculate a value for the cloud ice mixing ratio. So, when the air is supersaturated with respect to ice and the air temperature is below freezing, then most parameterization schemes assume that cloud ice forms when in the presence of ice nuclei. This assumption allows

observations of ice nuclei to be used as the basis for these schemes. Homogeneous nucleation that does not require ice nuclei is also included in some schemes (DeMott *et al.* 1994; Walko *et al.* 1995).

Fletcher (1962) derives a formula for the number of ice nuclei per unit mass of air in which

$$n_c = 0.01 \exp[0.6(273.16 - T)], \tag{7.37}$$

where n_c (m^{-3}) is the number of ice nuclei present at temperature T below freezing. Over the high plains of the USA, Bowdle *et al.* (1985) suggest a similar formula for the number of ice nuclei, but with a leading constant of 0.02 and an exponential factor of 0.3 instead of 0.6. Rauber (2003) shows that (7.37) is a reasonable fit to the available observations of ice nuclei concentrations for temperatures between −10 and −25 °C, although there is a fair amount of variability in the concentrations measured.

Dudhia (1989) uses the Fletcher expression for ice initiation, whereas Reisner *et al.* (1998) indicate that Fletcher's expression overestimates ice nucleation at very cold temperatures and so the value of T is not allowed to be below 246 K. The initiation rate of cloud ice is then described as

$$P_{ICE} = \left(\frac{m_i n_c}{\rho} - q_i\right)\frac{1}{\Delta t}, \tag{7.38}$$

where q_i is the cloud ice mixing ratio ($kg\,kg^{-1}$), m_i is the mass of a typical ice particle (1×10^{-12} kg), and Δt is the model time step (seconds).

Meyers *et al.* (1992) propose a different equation for ice crystal concentration, suggesting that

$$n_c = 1000 \exp\left[-0.639 + 12.96\left(\frac{q_v}{q_{vsi}} - 1\right)\right], \tag{7.39}$$

where q_{vsi} is the saturation water vapor mixing ratio over ice. This expression is used by Schultz (1995) to parameterize ice nucleation, but is not allowed if ice is already present. This is done because ice nucleation is a much slower process than deposition growth of ice crystals. Meyers *et al.* (1992) demonstrate the importance of the ice crystal concentration by comparing their formula for ice crystal concentration to that of the Fletcher (1962) formulation in a model simulation (Fig. 7.12). They also suggest that the Fletcher relationship probably overpredicts ice crystal concentrations for temperatures below −25 °C.

A third equation for ice crystal concentration is given by Cooper (1986) which provides for ice crystal concentrations that often are in between the values determined by Fletcher (1962) and Meyers *et al.* (1992). Thompson

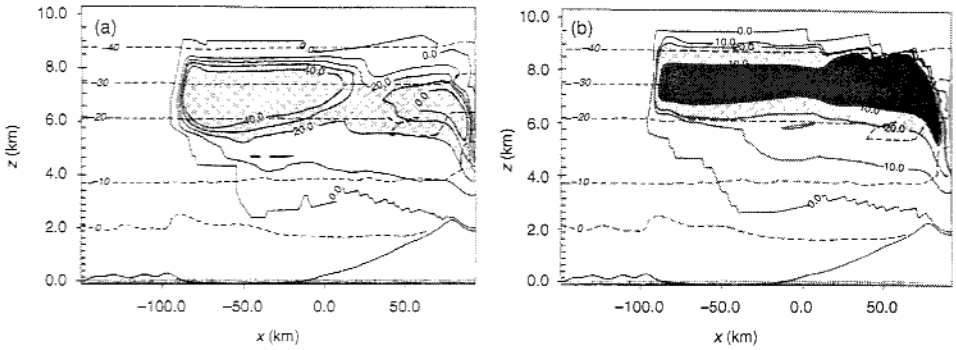

Figure 7.12. Simulated ice crystal concentrations at 4 h with (a) the Meyers formulation for ice crystal concentration and (b) a formula based upon the Fletcher (1962) equation. Maximum value in (a) is $76\,l^{-1}$ and in (b) is $900\,l^{-1}$. Isotherms are indicated every 10 °C. All distances are in km. From Meyers *et al.* (1992).

et al. (2004) use the Cooper (1986) relationship in their bulk microphysics parameterization.

7.4.6 Ice and snow aggregation

Ice crystals aggregate together to form snow, and snow particles may aggregate together to form graupel or hail (although graupel and hail formation and growth are strongly dominated by riming). These processes are often parameterized in a very similar fashion. The basic idea behind this parameterization is based upon the collision–coalescence process for cloud droplets to yield raindrops as proposed by Kessler (1969). Lin *et al.* (1983) suggest that the conversion rate from cloud ice to snow from aggregation of the cloud ice can be represented by

$$P_{AGGS} = 0.001 \exp[0.025(T - T_0)](q_i - q_{i\_threshold}), \tag{7.40}$$

where q_i is the cloud ice mixing ratio ($\mathrm{kg\,kg^{-1}}$), T_0 is the freezing temperature, and the threshold value for the cloud ice mixing ratio used is $1 \times 10^{-3}\,\mathrm{kg\,kg^{-1}}$. Dudhia (1989) follows Rutledge and Hobbs (1983), who develop a similar expression, namely

$$P_{AGGS} = \left[q_i - \frac{m(500\ \mu\mathrm{m})n_c}{\rho}\right]\frac{1}{\Delta t}, \tag{7.41}$$

where $m(500\,\mu\mathrm{m})$ is the mass of a 500 μm ice crystal (9.4×10^{-10} kg), and n_c is the ice nuclei concentration (7.37) from Fletcher (1962).

Graupel or hail formation from the aggregation of snow crystals can be defined in a very similar fashion. Lin *et al.* (1983) have

$$P_{AGGG} = 0.001 \exp[0.09(T - T_0)](q_s - q_{s\_threshold}), \tag{7.42}$$

where q_s is the snow mixing ratio, T_0 is the freezing temperature, and $q_{s\_threshold} = 6 \times 10^{-4}\,\mathrm{kg\,kg^{-1}}$. The temperature dependence of the rate coefficient has the same form as that used for the aggregation of ice crystals to form snow. The initiation of graupel through collisions of snow crystals is considered unimportant by Rutledge and Hobbs (1984), who only allow graupel to form from collisions between liquid water and ice.

Reisner *et al.* (1998) base their aggregation approximation on the study of Murikami (1990), and define the aggregation of ice crystals to form snow as

$$P_{AGGS} = \frac{q_i}{\Delta\tau_1}, \tag{7.43}$$

where

$$\Delta\tau_1 = -\frac{2\rho_i}{\rho q_i a_i E X} \log\left(\frac{(3\rho q_i / 4\pi\rho_i n_i)^{1/3}}{r_{S0}}\right)^3. \tag{7.44}$$

Here ρ_i is the density of ice, $E = 0.1$ is the collection efficiency, $X = 0.25$ is the dispersion of the fall velocity of cloud ice, $r_{S0} = 0.75 \times 10^{-4}$ m is the radius of the smallest snowflake, n_i is the predicted number concentration of cloud ice, and $a_i = 700$ is the constant in the snow fall speed equation. The size of the smallest snowflake in this parameterization is slightly more than three times smaller than the assumed snowflake size used in Rutledge and Hobbs (1983) and Dudhia (1989).

Finally, snow is produced in the Schultz (1995) scheme when cloud ice exceeds a specified content. Thus, he sets

$$l_s = (l_i - l_{i\_threshold}), \tag{7.45}$$

where $l_{i\_threshold} = 0.1 \times 10^{-3}\,\mathrm{kg\,m^{-3}}$.

7.4.7 *Accretion by frozen particles*

Accretion by frozen particles is the process by which precipitating frozen particles (snow, graupel, or hail) collect other ice or liquid particles as they fall. There are a number of different water forms that can be accreted by frozen particles. For example, graupel can accrete cloud ice, snow, rain water, and cloud water. The accretion by graupel or snow of rain water and cloud water is

commonly called riming. Riming dominates the formation and growth of graupel and hail. As with the accretion of cloud water by raindrops, the general derivation follows Kessler (1969) and it is assumed that a precipitating particle falling through a given layer sweeps out a cylindrical volume as it falls, thereby having a chance to collect all the droplets in its path. The basic derivation follows the same process as accretion of cloud droplets by raindrops discussed above and so is not repeated.

The rate of accretion by graupel/hail of cloud ice is represented in Lin *et al.* (1983) as

$$P_{ACGI} = \frac{\pi E n_{0g} q_i \Gamma(3.5)}{4\lambda_g^{3.5}} \left(\frac{4g\rho_g}{3C_D\rho}\right)^{1/2}, \tag{7.46}$$

where $E = 0.1$ is the collection efficiency of graupel for cloud ice, q_i is the cloud ice mixing ratio ($\mathrm{kg\,kg^{-1}}$), λ_g is the graupel slope parameter, ρ_g is the graupel density, n_{0g} is the graupel intercept parameter, and $C_D = 0.6$ is a drag coefficient for hail. A nearly identical expression is used for the accretion of cloud water by graupel (riming), but with a collection efficiency of 1.0 and q_i replaced by q_c in the equation. Houze (1993) indicates that the collection efficiency for riming is not well-known either from a theoretical or an observational perspective, but is thought to be very high and so an efficiency of unity is often assumed.

Some differences are found in the various expressions for accretion, largely owing to how the fall speed is defined. For example, Rutledge and Hobbs (1983) derive the accretion of cloud ice by snow as

$$P_{ACSI} = \frac{\pi\rho a_s q_i E n_{0s} \Gamma(b_s + 3)}{4\lambda_s^{b_s+3}} \left(\frac{p_0}{p}\right)^{0.4}, \tag{7.47}$$

where $E = 0.1$ is the collection efficiency for cloud ice by snow, and a_s and b_s are the constants in the fall speed equation for snow. Owing to the similar form of the fall speed equation, this expression is nearly identical to the accretion equation for cloud water by rain water as expected.

Additional terms are added when both species are falling, such as the accretion of snow by graupel or the accretion of rain by graupel (riming). For example, for the accretion of rain water by graupel, Lin *et al.* (1983) use

$$P_{ACGR} = \pi^2 E n_{0g} n_{0r} |\overline{V}_g - \overline{V}_r| \left(\frac{\rho_w}{\rho}\right) \left(\frac{5}{\lambda_r^6 \lambda_g} + \frac{2}{\lambda_r^5 \lambda_g^2} + \frac{0.5}{\lambda_r^4 \lambda_g^3}\right). \tag{7.48}$$

Thus, not only is the accretion rate a factor of the intercept and slope parameters for the two precipitation types, but also is a factor of the difference in

fall speeds. Some schemes use a polynomial fit to the fall speed relationship for raindrops, in which the fall speed is a function of the drop diameter, and this then alters the accretion rate equation. Murikami (1990) modifies this expression slightly to account for continued accretion when the mass-weighted fall speeds of the colliding hydrometeor species are similar, although Ferrier *et al.* (1995) find that this modification has little influence.

Unlike the accretion of cloud water by rain water, which can be complete and leave no cloud water behind, cloud ice typically remains within clouds that extend above the freezing level (Schultz 1995). Thus, Schultz checks to make certain that the cloud ice specific content of 0.001 kg m^{-3} remains once cloud ice is formed. His accretion equation is

$$P_{ACSI} = \frac{5}{\rho}\left(1 - \frac{273.1 - T}{50}\right) l_i l_s, \tag{7.49}$$

where the temperature dependence is related to the collection efficiency of the aggregation process.

Reisner *et al.* (1998) incorporate an equation for the rate of conversion from snow to graupel via accretion (riming) of cloud water. A so-called "three-body process" is parameterized in which the interaction of two habits produces a third, yielding

$$P_{AGGG} = 2\alpha\Delta t \frac{3\rho_0 \pi n_{0s} (\rho q_c)^2 E^2 \Gamma(2b_s + 2)}{8\rho(\rho_g - \rho_s)\lambda_s^{2b_s - 2}}, \tag{7.50}$$

where ρ_g and ρ_s are the densities of graupel and snow, respectively, E is the collection efficiency for snow collecting cloud water, and n_{0s} is the intercept parameter for snow. A more standard equation for the accretion of cloud water by snow is determined, as in Rutledge and Hobbs (1983), and any increase in the accretion of cloud water by snow that is not converted directly into graupel is used to increase the snow mixing ratio.

Finally, Schultz (1995) parameterizes an accretion rate for graupel as simply the specific content (kg m^{-3}) of the colliding particles multiplied together with a constant conversion parameter. Thus, graupel is allowed to accrete cloud water and snow.

7.4.8 Deposition

The growth of ice crystals, and also their sublimation to water vapor, are parameterized following Byers (1965). Ice crystal, snow, and graupel growth via deposition occur when the environment is supersaturated with respect to

ice. The treatment of deposition follows very closely the growth and evaporation of rain water and cloud water. However, the variety of shapes of ice crystals necessitates the diffusion process being handled in a different manner, since a simple spherical shape cannot be assigned. Thus, the diffusion of water vapor to a given crystal is approximated as if it is a current flowing to an object in an electric field. Following Rutledge and Hobbs (1983), the growth rate by vapor deposition of an ice crystal is defined as

$$\frac{dm}{dt} = \frac{C(S_i - 1)/\varepsilon_0}{A'' + B''}, \tag{7.51}$$

where

$$A'' = \frac{L_v}{K_a T}\left(\frac{L_s}{R_v T} - 1\right) \tag{7.52}$$

and

$$B'' = \frac{R_v T}{\chi e_{si}}. \tag{7.53}$$

Here ε_0 is the permittivity of free space ($8.854 \times 10^{-12}\,\mathrm{C^2\,N^{-1}\,m^{-2}}$), K_a is the thermal conductivity of air ($2.43 \times 10^{-2}\,\mathrm{J\,m^{-1}\,s^{-1}\,K^{-1}}$), χ is the diffusivity of water vapor in air ($2.26 \times 10^{-5}\,\mathrm{m^2\,s^{-1}}$), and e_{si} is the saturation vapor pressure for ice. Rutledge and Hobbs (1983) assume a hexagonal plate-like ice crystal shape, so that $C = 4D_I\varepsilon_0$, where D_I is the average diameter of the ice crystal. They then relate D_I to the mass of the plate-like ice crystal, which is computed from the cloud ice mixing ratio and the number of ice crystals specified from the formula of Fletcher (1962). Assuming a single size for all ice crystals, this yields an equation for the depositional growth of cloud ice,

$$P_{DEPI} = \frac{4\overline{D}_I(S_i - 1)n_c}{A'' + B''}. \tag{7.54}$$

A similar approach is taken by Koenig (1971), the results of which are used in the microphysics scheme of Reisner *et al.* (1998). This derivation yields a slightly different expression, in which the depositional growth of cloud ice is given as

$$P_{DEPI} = \frac{q_v - q_{vsi}}{q_{vsw} - q_{vsi}} a_1 (m_i)^{a_2} n_i \frac{1}{\rho}, \tag{7.55}$$

where q_{vsi} is the saturation vapor pressure for ice, q_{vsw} is the saturation vapor pressure for water, m_i is the mass of a pristine ice crystal ($m_i = q_i / n_i$), n_i is the

ice crystal number concentration, and a_1 and a_2 are temperature-dependent constants from Koenig (1971) that are used over a range from 0 to −35 °C.

A related approach is taken by Schultz (1995), who defines the depositional growth of ice crystals as a function of the supersaturation and the ice crystal mass already present in the atmosphere. Thus, he defines

$$P_{DEPI} = 25(l_v - l_{vsi})l_i, \tag{7.56}$$

where the rate is in terms of the specific content. These values are then converted back to mixing ratios after all the calculations are complete.

When snow is present in air that is supersaturated with respect to ice, then snow particles can grow by deposition as well. However, snow particles are not monodisperse and so one must again assume a distribution function. If an inverse exponential function is assumed for the snow size distribution, then the deposition growth equation can be integrated over all sizes to obtain (Rutledge and Hobbs 1983)

$$P_{DEPS} = \frac{4(S_i - 1)n_{0s}}{A'' + B''}\left[\frac{0.65}{\lambda_s^2} + 0.44\left(\frac{a_s\rho}{\mu}\right)^{1/2}\left(\frac{p_0}{p}\right)^{0.2}\frac{\Gamma\left(\frac{b_s+5}{2}\right)}{\lambda_s^{(b_s+5)/2}}\right]. \tag{7.57}$$

This expression for deposition is used by Reisner *et al.* (1998), except for neglecting the pressure correction term, and a very similar expression is used by Lin *et al.* (1983). Some of the differences in the expressions are due to different assumed particle shapes, with Lin *et al.* (1983) assuming spherical particles and Rutledge and Hobbs (1983) assuming hexagonal particles.

The deposition growth of graupel or hail yields expressions that are very similar to those for the deposition growth of snow, but with different intercept and slope parameters, slightly different constants related to the expressions for particle fall speed, and different coefficients related to particle ventilation factors.

A subtle but important factor to consider in the construction of microphysics parameterizations is the order in which the various physical processes are evaluated. For example, if cloud ice deposition is evaluated before snow deposition, and the saturation ratio is adjusted after each evaluation, then there is less vapor available for snow deposition in comparison to cloud ice deposition. Some schemes address this problem by evaluating all the terms at once, while others neglect it.

7.4.9 Melting

Calculations of the melting rates of hailstones and graupel are derived first by Mason (1956). A hailstone or graupel particle falling through air gains heat

from the environment via conduction and convection. If its surface temperature, assumed to be 0 °C during melting, is below the dewpoint of the environment, then additional heat may be produced by the condensation of water vapor on the surface of the particle. This heat is then used to melt the particle. In contrast, if the environment is very dry the particle may lose heat due to evaporation. Similar processes occur for snow. Assuming an inverse exponential distribution for the snow size distribution and integrating over all sizes yields an expression for the rate of the melting of snow (Lin *et al.* 1983)

$$P_{MLTS} = -\frac{2\pi}{\rho L_f}[K_a(T - T_0) - L_v\varphi\rho(q_{vsi}(T_0) - q_v)]n_{0s} \times \left[\frac{0.78}{\lambda_s^2} + 0.31S_c^{1/3}\Gamma\left(\frac{b_s+5}{2}\right)c^{1/2}\left(\frac{\rho_0}{\rho}\right)^{1/4}\frac{1}{\nu^{1/2}\lambda_s^{(bs+5)/2}}\right] - \frac{c_w(T - T_0)}{L_f}(P_{SACW} + P_{SACR}), \tag{7.58}$$

where L_f is the latent heat of fusion, T is the environmental temperature (K), T_0 is the temperature of freezing, K_a is the thermal conductivity of air, φ is the diffusivity of water vapor in air, $q_{vsi}(T_0)$ is the water saturation mixing ratio at T_0, ν is the kinematic viscosity of air, c_w is the specific heat of water, and P_{SACW} and P_{SACR} are the accretion of cloud water and raindrops, respectively, by the falling snow. The first term on the right-hand side with $K_a(T - T_0)$ represents the conduction of heat from the air, while the second term represents the heat added from condensation on the surface of a melting particle (Musil 1970). Rutledge and Hobbs (1983) and Reisner *et al.* (1998) use very similar expressions, but neglect the condensation effects. Mason (1956) shows that the distance hail falls before melting completely is reduced by several hundred meters when condensation effects are not included.

One of the differences between melting hail and graupel is that hail particles, being of solid ice density, shed all meltwater immediately. However, as graupel is composed of low-density rime (i.e., it contains air spaces between frozen droplets), graupel particles initially soak in the meltwater and subsequently shed the excess meltwater after the rime has saturated. Such effects present an additional challenge to the explicit prediction of microphysical variables.

Dudhia (1989) assumes that all frozen particles melt as they pass through the freezing level, and so the melting rate is directly proportional to the precipitation mixing ratios. Cloud ice only melts if the grid-scale vertical motion is subsiding, since cloud ice follows the model flow field and has no relative fall speed. Schultz (1995) assumes that the melting rate is a function of temperature only, with increasing rates as the temperature increases above freezing. He also

checks to be certain that melting does not cause the environmental temperature to go below freezing. Rutledge and Hobbs (1984) and Ferrier (1994) both account for the heat transfer that enhances melting as cloud water and rain are collected by the falling graupel particles. Model simulations indicate that melting is an important process that influences the development and structure of midlatitude convective systems (Tao *et al.* 1995).

7.5 Discussion

While this discussion of the various microphysical interaction terms is not complete, and has left out a number of terms, the general procedures for calculating the rates of conversion are similar across all schemes and processes. Thus, the preceding discussion gives a flavor of the typical parameterization methods and the included physical processes. It is important to realize that the various microphysical schemes tend to differ significantly in the number of interactions between the microphysical particles that are represented (Fig. 7.13). Some schemes are fairly simple and only account for a handful of interactions, while others are much more sophisticated. The scheme available or selected for use in a given model likely depends upon the phenomena

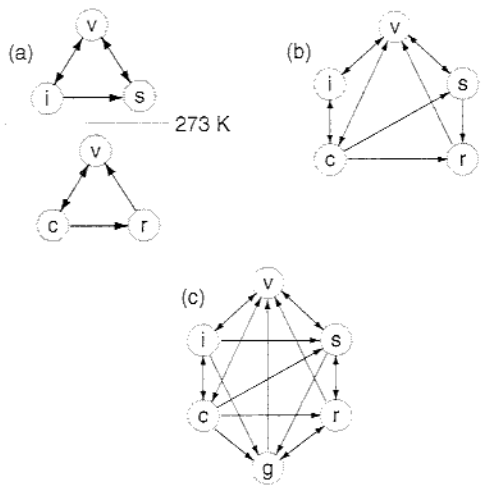

Figure 7.13. Illustration of the microphysical processes available in (a) Dudhia (1989), (b) Reisner *et al.* (1998), and (c) Lin *et al.* (1983). Arrows denote the direction in which the particles are allowed to interact. The letter v denotes water vapor, i denotes ice, s denotes snow, c denotes cloud water, r denotes rain water, and g denotes a combination of graupel and hail. The line in (a) marked 273 K denotes the freezing level, with frozen precipitation processes only above this level and warm precipitation processes only below this level.

one would like to forecast or simulate, and the availability of computational resources to run the scheme in a timely manner.

Numerical simulations using bulk microphysics schemes have been quite successful in reproducing many observed features of individual clouds and cloud systems. For example, Ziegler *et al.* (1997) show that a model with 1 km minimum grid spacing can at times reproduce the storm-scale features of convective storms near the dryline (Fig. 7.14), beginning with swelling and towering cumulus along the dryline that develop over time into a thunderstorm with

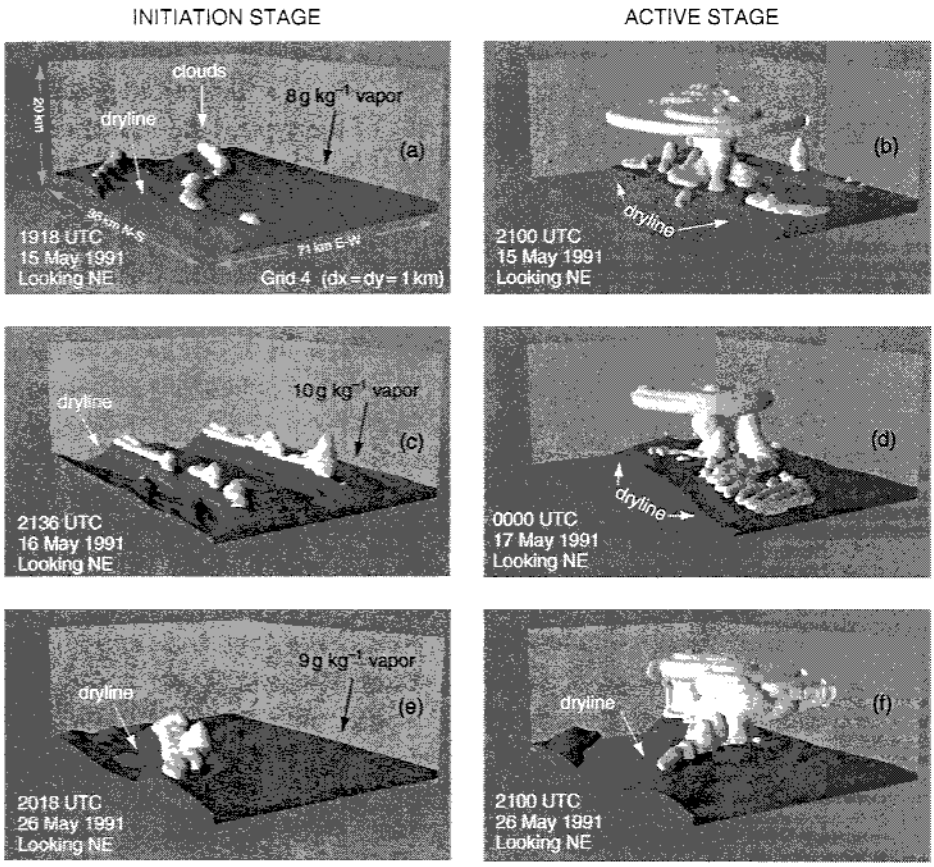

Figure 7.14. Surfaces of cloud (white) and constant water vapor mixing ratio (gray) in perspective view at the initiation and active stage of simulated dryline convection from three days during 1991 using a multigrid cloud-scale model. The depictions are valid at (a) and (b) 1918 and 2100 UTC 15 May, (c) and (d) 2136 UTC 16 May and 0000 UTC 17 May, and (e) and (f) 2018 and 2100 UTC 26 May, respectively. The values of water vapor mixing ratio isosurfaces are indicated in each initiation stage figure. Simulations shown here employ a bulk single-moment warm rain parameterization. From Ziegler *et al.* (1997).

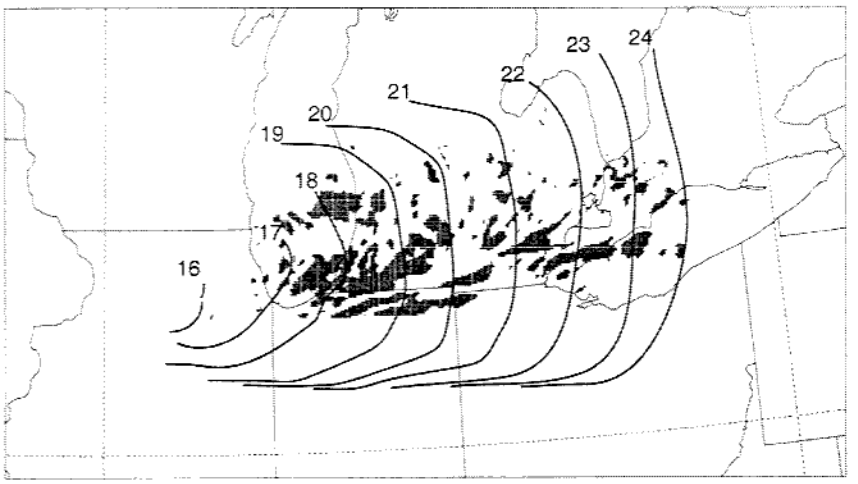

Figure 7.15. Approximate hourly location of a surface gust front (solid lines) associated with a simulated derecho-producing convective system and grid points from the 2.22 km grid that have winds $\geq 26\,m\,s^{-1}$ at the surface through the 24 h simulation time. Simulation shown here uses a bulk single-moment ice microphysics parameterization. From Coniglio and Stensrud (2001).

overshooting tops and a spreading anvil. Coniglio and Stensrud (2001) simulate a derecho-producing convective system and find that the swaths of severe surface winds ($\geq 25\,m\,s^{-1}$) produced by the model are very realistic in their distribution (Fig. 7.15). Lee and Wilhelmson (1997) use a bulk scheme to reproduce Florida thunderstorms with land spouts (Fig. 7.16). Finally, Bryan *et al.* (2003) use a warm-rain-only bulk scheme at very small grid spacing (125 m) to reproduce very detailed features in a squall line that contrast with the much smoother fields seen when using 1 km grid spacing (Fig. 7.17). Thus, it is clear that models with bulk microphysical schemes can reproduce many of the observed features of deep convection.

However, we are learning that there are numerous limitations to bulk microphysics schemes that only predict the mixing ratio. Gilmore *et al.* (2004a) nicely describe several of these limitations. While the constants empirically derived for most of the rate equations involving microphysical processes are fairly well specified through a history of observational studies (e.g. Pruppacher and Klett 2000), it is widely regarded that there exists a range of possible values for two graupel parameters that are defined a priori and held constant during the model simulations. These two parameters are the intercept parameter for the graupel inverse exponential size distribution and the graupel density. Reasonable selections for these two parameters can yield substantial

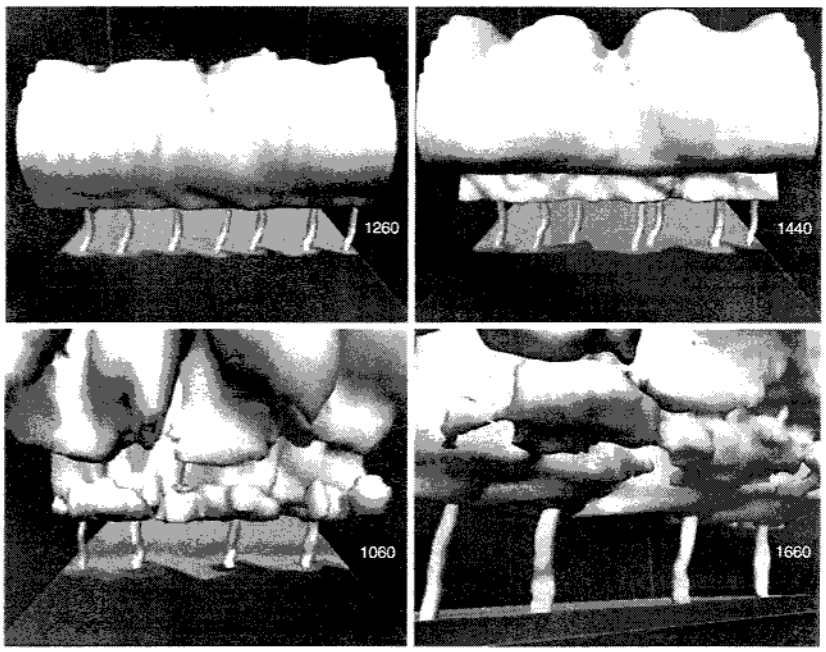

Figure 7.16. Three-dimensional renderings of model simulation output showing the evolving ensemble of leading-edge vortices, storms, and outflow boundaries at 21 (upper left), 24 (upper right), and 31 min (bottom panels) into the simulation. White vertical tubes indicate a vertical vorticity in excess of $0.1\,s^{-1}$. The shades along the surface depict the temperature of surface outflow (darker shades denote colder temperatures). Cloud isosurfaces shown for $0.2\,g\,kg^{-1}$ values of cloud water. Simulations shown employ only bulk single-moment warm rain processes following Kessler (1969). From Lee and Wilhelmson (1997).

and operationally important differences in numerical simulations of thunderstorms in terms of storm structure, severity, and intensity (Fig. 7.18).

In actual thunderstorms, the value of the intercept parameters n_{0g} can vary widely within a single storm and among storms (Fig. 7.19) in the same background environment (Dennis *et al.* 1971; Federer and Waldvogel 1975; Spahn 1976; Knight *et al.* 1982). Values of n_{0g} suggested by observations range from 10^3 to 10^5 for hail and as high as 10^{10} for graupel (Knight *et al.* 1982). The density of graupel particles also varies significantly, and can range from 50 to $890\,kg\,m^{-3}$ while hail density varies from 700 to $900\,kg\,m^{-3}$ in observed storms (Pruppacher and Klett 2000).

The values of n_{0g} and ρ_g are important because they influence many of the microphysical process parameterization schemes. For example, as n_{0g} and ρ_g increase, the mass-weighted terminal velocity decreases. This is because the

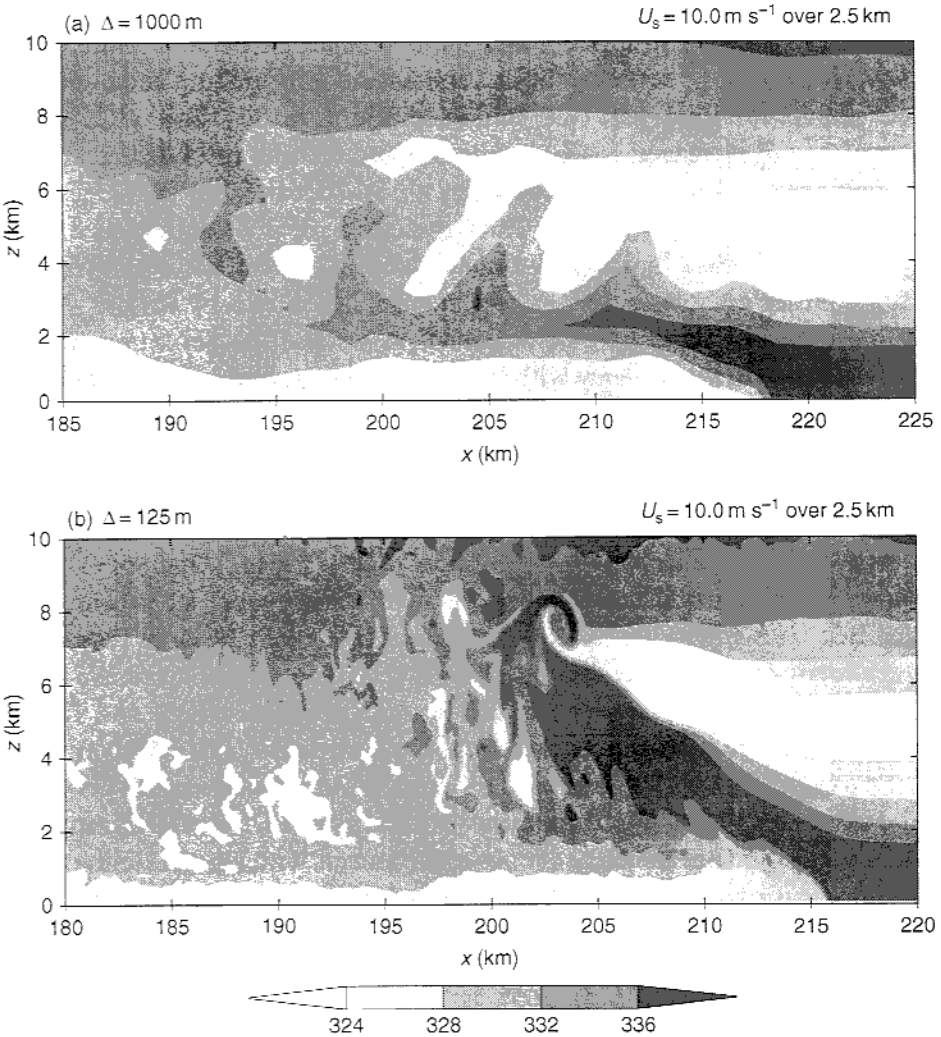

Figure 7.17. Squall line-normal cross-sections of equivalent potential temperature (K) from weak shear simulations at 180 min using (a) 1000 m grid spacing and (b) 125 m grid spacing. Cross-sections taken along $y = 49$ km. Warm rain processes only following the bulk single-moment approach of Kessler (1969). Note the dramatic change in squall line structure as the grid spacing is reduced. From Bryan *et al.* (2003).

particle distribution becomes more heavily weighted towards the smaller particles, which fall more slowly. Changes in fall speed influence the vertical distribution of the graupel particles over time. As ρ_g increases, the graupel particle distribution has fewer larger particles and becomes more heavily weighted towards smaller particles. In addition, the mass-weighted fall speed

is applied uniformly to each particle in the distribution, such that small graupel particles are falling too quickly and large graupel particles are falling too slowly. Then as n_{0g} increases, both sublimation and melting rates increase since smaller graupel particles sublimate more readily and melt faster. However, as ρ_g increases, both sublimation and melting rates decrease, since the diameters of denser graupel particles are smaller because the slope parameters are larger following (7.5). Thus, these two parameters influence many of the microphysical process parameterizations and in ways that can be at times either complementary or destructive. As shown by Ziegler (1988), the intercept and slope parameters must, in general, be permitted to vary independently for consistency with independently varying concentration and mixing ratios.

It is clear that the values of both n_{0g} and ρ_g influence the mean properties of the graupel distribution in the model forecasts, and feed back to influence the precipitation amounts, downdraft intensities, and general evolution of simulated thunderstorms as shown by Gilmore *et al.* (2004a). One approach to avoiding or minimizing these limitations is to include more ice precipitation categories, with the individual microphysical rate terms broadly resembling those already discussed. Straka and Mansell (2005) describe a scheme in which there are two liquid categories (cloud water and rain water), and ten ice categories that are characterized by habit, size, and density. The larger number of ice categories allows for a range of different particle densities, fall velocities, and greater complexity of precipitation growth histories, hopefully promoting the ability to simulate a variety of convective storms with limited tuning of the microphysical parameters. Another approach is to utilize snow and graupel intercept parameters that depend upon either the mixing ratio (Swann 1998; Thompson *et al.* 2004) or the temperature (Thompson *et al.* 2004) within a single-moment bulk microphysics scheme.

In a wintertime environment, results from a simulation of an orographic precipitation event indicates that the bulk microphysics parameterization used produces too much supercooled cloud water aloft and too little snow compared to observations (Colle *et al.* 2005a). While the total rainfall is reasonably well predicted, observations suggest that snow deposition and aggregation dominated the generation of surface precipitation in contrast to the model results that indicate riming and cloud water accretion being dominant. Colle *et al.* (2005a) further show model sensitivity to the slope intercept value for the snow size distribution, further emphasizing the challenges to accurate bulk microphysics parameterizations. Other comparisons of model simulations and observations of microphysics parameters by Garvert *et al.* (2005) and Colle *et al.* (2005b) indicate that while the overall simulation of the cloud field is

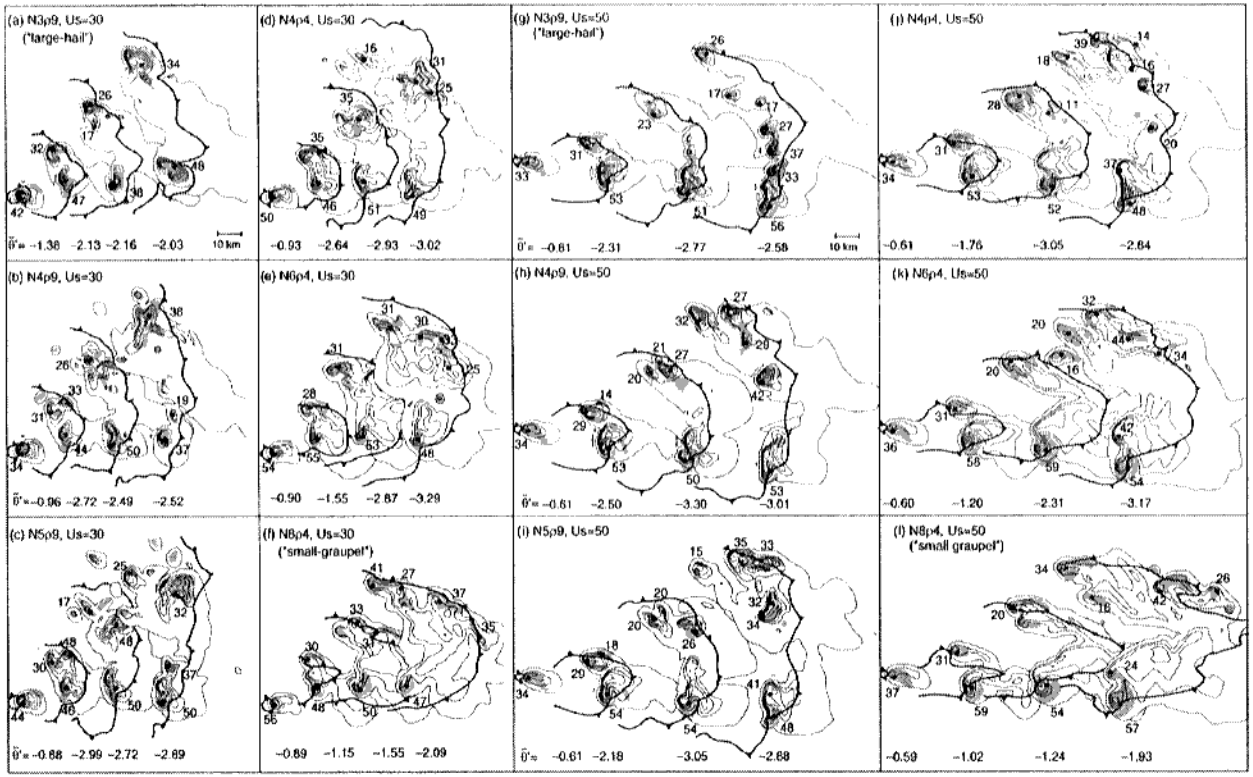

Figure 7.18. Evolution of mid-level thunderstorm structure shown at 30, 60, 90, and 120 min for 30 m s^{-1} of half-circle hodograph shear in (a)–(f) and 50 m s^{-1} of half-circle hodograph shear for (g)–(l). Results from six variations in the bulk three-class single-moment microphysics scheme are illustrated. The total precipitation mixing ratio at $z = 4.75$ km is shown using 2 g kg^{-1} intervals starting at 1 g kg^{-1}. Regions of updraft greater than 5 m s^{-1} at this level are shaded. Maximum updraft values indicated in m s^{-1}. The barbed line shows the position of the surface gust front. The minimum area-averaged potential temperature for each time is shown at the bottom of each panel. Cases are labeled *Naρb*, where *a* indicates the exponent in the slope intercept ($n_{ox} = 4 \times 10^{a}$ m^{-4}), and *b* is the first digit in the graupel density, *b*00 kg m^{-3}. Thus, *N3ρ9* has a slope intercept of 4×10^{3} m^{-4} and a graupel density of 900 kg m^{-3}. From Gilmore *et al.* (2004a).

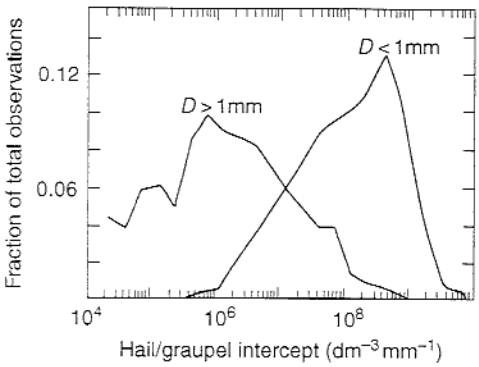

Figure 7.19. Relative frequency of the hail and graupel slope intercept parameter n_{0g} observed during the National Hail Research Experiment. "$D > 1$ mm" and "$D < 1$ mm" denote the two distributions for these different sized groups of particles. From Gilmore *et al.* (2004a) as adapted from Knight *et al.* (1982).

reasonable, the parameterization overpredicts cloud liquid water over the windward slopes, produces excessive snow, and misclassifies snow as graupel.

Beyond including more hydrometeor categories in a scheme, another improvement is to include independent conservation equations for the mixing ratio and the number concentration, and their tendencies. Examples of this class of double-moment microphysics schemes are found in Ziegler (1985), Ferrier (1994), Meyers *et al.* (1997), and Reisner *et al.* (1998), while a triple-moment scheme is developed by Clark (1974). As with turbulence closure (discussed in Chapter 5), it is hoped that parameterizing the microphysical processes at higher moments leads to better predictions of the variables, such as accumulated precipitation and downdraft intensities which are most important to weather forecast users.

While microphysical processes are known to be important to climate, through the indirect aerosol effects (Twomey 1977; Albrecht 1989) and other cloud–radiation interactions, climate models generally do not use such detailed explicit microphysical parameterizations since the grid spacing in these models is large. However, as the grid spacing of climate models continues to decrease, there will be a need to include more detailed explicit microphysics schemes in these models at some point in time.

7.6 Questions

1. Plot the saturation ratio S for pure water as a function of the cloud droplet radius.
2. In the calculation of the saturation ratio S, include the effects of a solute and replot the curve for various amounts of solute mass. Assume the solute is sodium chloride

(NaCl) and that the solute has mass values of 1×10^{-16}, 1×10^{-15}, 1×10^{-14}, 1×10^{-13}, 1×10^{-12}, 1×10^{-11}, and 1×10^{-10} g.

3. Plot the Marshall–Palmer raindrop size distributions for $n_{0r} = 1 \times 10^{-4}\,\mathrm{m}^{-4}$, $\rho = 1.0\,\mathrm{kg\,m}^{-3}$, and rain water mixing ratios between 1×10^{-8} and $1 \times 10^{-3}\,\mathrm{kg\,kg}^{-1}$. Plot the curves at regular intervals of the rain water mixing ratio. At what value of the rain water mixing ratio do more than 10 drops with diameters greater than 5 mm occur for a bin size of 1 mm?
4. Calculate the autoconversion rate using the Kessler, Lin *et al.*, and Tripoli and Cotton expressions over a likely range of cloud water mixing ratios. How large are the differences in autoconversion rates?
5. Derive the Kessler form of the accretion equation (7.23)–(7.25). Show all steps.
6. Compare the Kessler, Tripoli and Cotton, and Schultz accretion rates. Assume that $a = 841.996\,\mathrm{m}^{1-b}\,\mathrm{s}^{-1}$ and $b = 0.8$ in the fall speed equation. At what value of the rain water mixing ratio are the schemes most different?
7. Calculate the distance a raindrop can fall in an environment with a constant relative humidity of 80% and a constant temperature of 278 K for drop sizes of 0.5, 2, and 5 mm. Assume the ventilation factor $F = 1$ to simply the calculations. Assume that the thermal conductivity $K_a = 2.5 \times 10^{-2}\,\mathrm{J\,m}^{-1}\,\mathrm{K}^{-1}\,\mathrm{s}^{-1}$ and that the diffusivity of water vapor in the air $D_{diff} = 2.4 \times 10^{-5}\,\mathrm{m}^2\,\mathrm{s}^{-1}$.
8. Compare ice aggregation to form snow rate equations from Lin *et al.*, Dudhia, and Murikami for a reasonable range of values for the ice mixing ratio. State any assumptions made. How large are the differences in the snow production rate from these three approaches?